254

Egypt. J. Chem. **Vol. 65**, No. 4 pp. 449 - 474 (2022)

Egyptian Journal of Chemistry

http://ejchem.journals.ekb.eg/

Induced effects of gamma irradiation on activated carbon derived from *Hyphaene Thebaica* husks as a potential adsorbent for Chlorpyrifos pesticide-air purification

M.S. Yahia [a], H. F. Youssef[b], A. S. Elfeky[a], M. B. Awad[a], A. S. Elzaref[a*]

[a] *Chemistry Department, Faculty of Science, Al-Azhar University, Nasr City 11884, Cairo, Egypt.*
[b] *Inorganic Chemical Industries and Natural Resources, National Research Centre, El-Behouth St. 12622, Cairo, Egypt*

Abstract

In the current study, Doum palm husk of *Hyphaene Thebaica* (HT), a local agrow-waste, was utilized as a new source for the production of activated carbon (HT-AC). The thermally prepared adsorbent was chemically activated by phosphoric acid aqueous solution and exposed to γ-ray at doses of 2.5-10 Grays for capacity enhancement. Characterization of the obtained products were tested using FT-IR, SEM-EDX, XRD, BET and Raman spectroscopy.Thecarbonspecies were then utilized in the ambient air purification from the (chlorpyrifos) O,O-Diethyl O-(3,5,6-trichloropyridin-2-yl) phosphonothioate,(trade name, Ictafos) pesticideair pollutant. Results showed the development of very high surface area of 1439, 1702 and 1561m^2/g for the parent HT-AC and its HT-AC$_{2.5Gy}$ and HT-AC$_{5\ Gy}$ irradiated forms, respectively. The XRD, FT-IR and Raman testing of the carbons indicated better-organized structure of the sample subjected to the least gamma dose of 2.5Gy than the other irradiated versions. The experimental and theoretical results clarified the best fitting of pseudo-first-order model in describing the Chlorpyrifos sorption reaction. Thermodynamic analysis revealed physical sorption of the hazardous material onto the surfaces of the activated carbons with exothermic process of non-spontaneous nature. Experimental kineticspresentedthat,HT-AC$_{2.5Gy}$hadexcellent fitting to the Langmuir isotherm model, wherein the adsorption was proceeded in a monolayer manner with a uniform surface energy. Conversely, Freundlich isotherm was perfectly fitted to the original HT-AC and HT-AC 5Gy, where the multilayer and heterogeneous adsorption mechanism was exhibited

Keywords: Activated Carbon, *Hyphaene Thebaica* husk, Gamma Irradiation, Chlorpyridos-air purification, Adsorption process

1. Introduction

Hyphaene Thebaica (HT) is a kind of palm tree (doum palm) with eatable oval fruit; it grows in Upper Egypt and the whole northern half of Africa. The fruit (Dum) is being traded by street snack dealers and herbal shops, occasionally; sweetened and sold as a cold juice drink. Actually, it has pharmacological and nutritional effects that made it useful in treating some diseases such as bilharzias and its tea is considered as a healthy natural source for diabetic patients, as well as a traditional medicine for hypertension treatment[1]. As a result of these numerous uses, many tons of the husk remain as

agricultural waste, in Aswan Governorate, Upper Egypt, Dom palm waste is burned and causes serious environmental pollution which can be exploited and utilized since it resembles the coconut shell in terms of shape and nature and can be converted into activated carbon (AC) for absorbency. In this context, the shell material is pre-treated before the carbonization and activation process to improve the output of the produces AC, followed by chemical activation for more product efficiency.

Generally there is a wide variety of adsorbents with their own special properties(e.g., active carbon, zeolites[2], metal organic frameworks (MOF)[3], have been used due to their porosity and high surface

area in adsorption process, AC is one of the most common adsorbents applied for gas capture due to its clear porous nature, efficiency, availability and reusability[4]. In addition, high surface area[5], verities of pores[6, 7], excellent mechanical properties[8, 9], very reactive surface characteristics [10], better adsorption capacity and reliable physiochemical stability are other versatility properties it possesses [11, 12].

Globally, air pollution related to volatile organic compounds (VOCs) constitutes one of the most fatal environmental challenges in modern life. Most of such pollutants are sourced from the comprehensive and unwise utilization of pesticides worldwide, particularly in developing countries that are consuming much of it for improving crop yields and controlling agricultural pests [13]. These pesticides encompass organophosphorus, organchlorine, carbamates, anilines, ureas and pyrethroids. Organ phosphorus pesticides are the most widely used, amounting to several billion US dollars annually, including the insecticide ethion and (Chloropyrifos) O,O-Diethyl O-(3,5,6-trichloropyridin-2-yl) phosphorothioate [14].

Chlorpyrifos (commercially known as Ictafos, or simply as (CPF) is one of the most organo-phosphorous insecticides that are frequently applied in a regular manner all over the world for protecting many agricultural fruits, vegetables, ornamentals and trees from the harmful effects of insects[15]. CPF enters the environment through direct application to control ticks on cattle and as a spray to fight crop pests, lawns, domesticated animals, and in the home and workplace. The usage of CPF requires careful management due to a variety of demonstrated effects on non-target organisms, including aquatic pollinators and humans[16]. Adverse health effects can be mentioned on exposure to CPF, containing the developing of the nervous system, as an irreversible inhibitor of acetylcholinesterase and it can cause effects on the mammalian brain[17, 18].Various studies claim that prenatal exposure to the said substance can lead to autism, low birth weight, attention deficit issues and other behavioural disorders. It is true that, Chlorpyrifos transforms into chlorpyrifos Oxon in the atmosphere, which can also be 1000 times more harmful and can induce acute cholinergic neurotoxicity in organisms[19].

Improved performance of removing small amounts of various pesticide components with AC-modified

by gamma irradiation has been reported by some authors, who referred to a relative increase in the adsorbent surface area[20].Thus, for more efficient absorption of VOCs, avast surface area of activated carbon is obviously needed[21]. In gas filtration systems, systems containing fixed-bed reactor are usually employed, owing to low energy consumption and the zonal uptake properties, where there is a gradual adsorbent saturation, starting from the vicinities near the gas inlet and inward up to the complete adsorption process. Therefore, greater penetration of the adsorbent in the state of equilibrium is guaranteed[22], and parameters such as concentration of adsorbate, rate of gas flow, the mass of adsorbent, and the applied temperature are to be relevantly examined.

This work aims to synthesize and characterize an activated carbon adsorbent based on the local kernel shell of _Hyphaene Thebaica_ (HT). The primary product (AC) will be treated using different doses of gamma rays in the range of 2.5 to10Gy to give HT-AC irradiated species to be used as efficient porous materials for ambient air purification from Chlorpyrifos hazard. Characteristics of the prepared samples and the effect of adsorption conditions such as dose of adsorbent, Chlorpyrifos concentration, flow rate, and sorption temperature are to be tested.
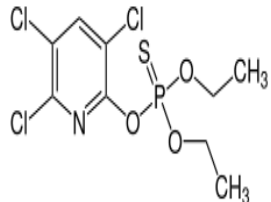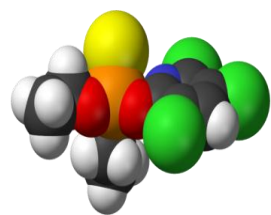
2. Experimental
2.1. Materials

All chemicals/reagents (H_3PO_4 and HCl) were purchased from Fisher scientific, (o-Phosphoric Acid, 85% -Hydrochloric acid 37%,specific gravity 1.8, laboratory reagent grade). The adsorbate, the pesticide effluent, is a commercial Chlorpyrifos (48%), that has $C_9H_{11}Cl_3NO_3PS$ chemical formula and is provided by ICCTA - International Co. for chemicals & trade agencies. Table 1shows the chemical structure and physical properties of chlorpyrifos[23].

2.2. Experimental methods
2.2.1. Preparation of the chemically-treated parent adsorbent (TH-AC)

Prior to the carbonization process, different pre-treatment steps including; washing, drying, raw sizing/grinding and sieving were carried out. The doum kernel was eliminated, then the husk was washed and soaked well in deionized water, to remove any contaminating impurities such as dust and water-soluble materials.

_____

Table 1: physical and chemical properties of Chlorpyrifos

CAS no.	2921-88-2	Chemical structure
Chemical formula	$C_9H_{11}Cl_{l3}NO_3PS$	
Preferred IUPAC name	O,O-DiethylO-(3,5,6-trichloropyridin-2-yl) phosphonothioate	
Molecular weight	350.57	
Melting point	41–42°C	
Boiling point	Decomposes at ~160°C	
Density at 43.5°C	1.398 g/cm^3	
Water solubility at 20°C	0.7 mg/L	
Water solubility at 25°C	2.0 mg/L	
Organic solvent solubility	79% w/w in isooctane, 43% w/w in methanol	
Partition coefficients	Log K_{ow}4.82, Log K_{oc}3.73	
Vapor pressure at 20°C and 25°C	1.87×10^{-5} mm	
Henry's law constant at 25°C	1.23×10^{-5} atm-m^3/mol	
Conversion factors at 25°C	1 ppm = 14.3 mg/ m^3 1 mg/ m^3 = 0.07 ppm	$C_9H_{11}Cl_{l3}NO_3PS$

For the moisture removal, the clean waste was then dried in an electric oven at 105 °C for 12 h to facilitate easy sizing and crushing to granules. Dry and clean raw husk was then cut, crushed and sieved to a particle size range of 1.5-2 mm. For chemical activation, the material was soaked in phosphoric acid (H_3PO_4) aqueous solution (conc.60 %) with 1:3 ratio (w/w) and has been shaken for 2h[24]. The mixture was then dehydrated overnight at 105 °C in an electric oven and the chemically treated husk was then thermally activated using a laboratory horizontal tubular furnace (CARBOLIT) at 700∘C with a constant heating rate of 10 ∘C/min, in the presence of reducing environment of purified nitrogen (99.99%) with flow rate 150 cm3/min for 2 h. The produced activated carbon (HT-AC) was kept inside the furnace to cool down up to room temperature, after which it was washed with 0.1 M HCl, followed by hot distilled water several times up to pH 6–7 for the filtrate solution. The final preparation step was to be finished dry the product at105 °C/24h in the oven and finally to store it in a closed container. Figure 1 represents
a schematic diagram for the preparation process of HT-AC from its raw source.

2.2.2. Modification process using Gamma-irradiation (TH-AC 2.5-10 Gy)

The prepared TH-AC product was subjected to direct surface alteration by applying different doses of Gamma rays in the range of 2.5-10Gy. The process was carried out by means of the instruments of the calibration unit of the radiological and chemical calibration branch (CRCB) of the main defense chemical laboratories of Egypt (MDCL), under the following conditions; 23°C and 60% relative humidity and a Cesium 137 source activity of 5.2 x1013 Becquerel. The total doses received were recorded by a dose meter radiation unit, and the irradiated samples were encoded as TH-AC$_{2.5-10Gy}$.

2.3. Dynamic adsorption processing

For determining the optimal adsorption conditions, the Chlorpyrifos sorption (in the gas phase) has been processed using fixed bed reactor, made up of packed column of the previously prepared irradiated HT-AC (2.5, 5, 7.5& 10Gy) materials, under atmospheric pressure with air as pesticide gas carrier and flow rates of 0.3–0.6 L min^{-1}, on sample amounts in the 0.25 – 1.0 g range. The concentrations of the Chlorpyrifos, in the gas phase, at the system inlet were ranging from 40 to 70 ppm at controlled temperatures of 18-42 °C. For preparing the exact air

_____

doses, 0.1- 0.3 ml of the Ictafos(48%) was diluted with 250 ml of distilled water and transferred to a 1000 ml round flask to be positioned in the thermostat which will be then adjusted to the desired temperature.

Experimentally, The CPF was continuously introduced to the gas phase using an air pump with an output of 2.5 L.min-1, using the bubbling technique where the airflow rate was determined using a volumetric flow meter. Meanwhile, the pesticide concentrations in the gas phase inlet and outlet were measured by a gas detector equipped with a PID sensor which has nonstop monitoring capability for volatile organic compounds (VOCs) [25, 26], via applying a photo-ionization detector (RAE Systems, MultiRAELite, lamp value 10.6eV).

The capacity of the prepared materials in adsorbing the hazardous gas was evaluated by calculating the difference in concentration of the pesticides gas before and after passing through the adsorption tube. The measurements were taken frequently with 1 min. time intervals.
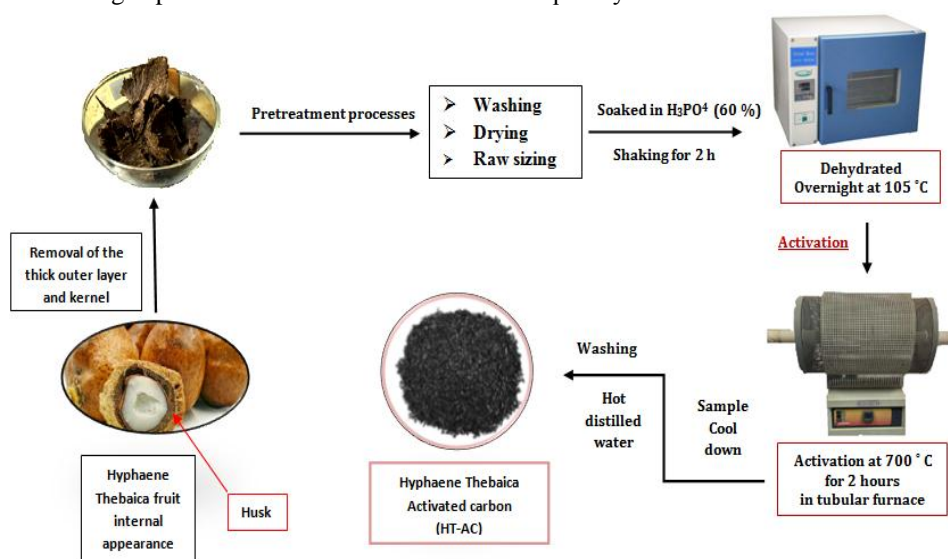

Figure 1: Schematic presentation for the preparation of activated carbon (TH-AC) from *Hyphaene Thebaica* (Doum palm)

2.3.1. Measuring the capacity and efficiency of adsorption

The following equation was used to determine the dynamic adsorption capacity:[27]

$$q = F/m \int (C_{in} - C_{out}) \, dt \text{-------------------(1)}$$

The integrated shape of the Eq. (1) may be defined as: $q_t = \sum_n^0 [F/m (C_{in} - C_{out})] \Delta t \text{--------------(2)}$

where, q_t (mg. g^{-1}) is the Chlorpyrifos adsorption capacity, i.e., the amount of pesticide adsorbed to the activated carbon. According to the Eq. (1), integrated by t = 0 through t (min); m (g) is the adsorbent dose; F (L.min^{-1}) is the gas flow rates; n is the sample number; C_{in} (ppm) and C_{out} (ppm) are the input and exit gas concentrations, respectively.

$q_t = q_e$ is achieved in the adsorption process when the equilibrium time (t_e) is reached, and refers to the capacity for equilibrium adsorption.

The adsorption efficiency is given as:

$$(R \%) = \frac{C_{in} - C_e}{C_{in}} \times 100 \text{--------------------------(3)}$$

Where, C_{in} (ppm) and C_e (ppm) are the inlet and equilibrium concentrations of the pesticide in the gas phase, respectively.

2.4. Characterization studies

For detecting any change in the surface functional groups of the prepared samples; raw and irradiated, the portable FT-IR, manufacturer by Bruker Optik GmbH was used at room temperature in the spectral range of 400-4000 cm-1. A Scanning Electron Microscope, model "SEM, FEI inspect S" with Energy-Dispersive X-ray Spectrometer (EDX), High-vacuum 200V – 30kV up to 2μA was used to monitor the original and modified microstructures of all samples before and after pesticide loading. EDX detector was employed to analyze the distribution of

_____

pollutant ions onto the adsorbent surfaces before and after the uptake process. The Raman analysis was conducted via Raman Microscopy of SENTERRA II model, Bruker Optik GmbH, Research-grade. The experimental conditions were as follows: excitation light source wavelength 532 nm, resolution 4 cm^{-1}, scanning time 2s, and measurement range 0 –4000 cm^{-1}, and laser power of 25 mW. The specific surface area for the adsorbents was determined using NOVA e-Series analyzer, utilizing the BET surface area results using the classical helium void volume method.

3. Results and discussion

3.1. Characterization of Prepared Activated Carbon

3.1.1. X-Ray Diffraction

The possible change in the structural nature of both the as-prepared and the irradiated products were examined and their collected XRD patterns were given in Figure 2 .Obviously, the XRD profile of all treated (TH-AC$_{2.5-10Gy}$), and untreated (HT-AC) precursor, were sharing the presence of two main broad undifferentiated peaks, centered around 2θ ≈24° and 43°, corresponding to the diffractions of (002) and (100/101) crystallographic planes, in respective order. The previous diffractions signify the interlayer spacing (Lc) and the diameter of the micro crystallite (La)[28],or simply, the height of the stacked layers, and the crystallites lateral sizes (width), respectively[29].AS shown In Figure 2, the 002-diffraction indicated higher intensity for the HT-AC and its irradiated version at 2.5Gy, which may mark an ordering and probable building up of some aromatic sheets[29].
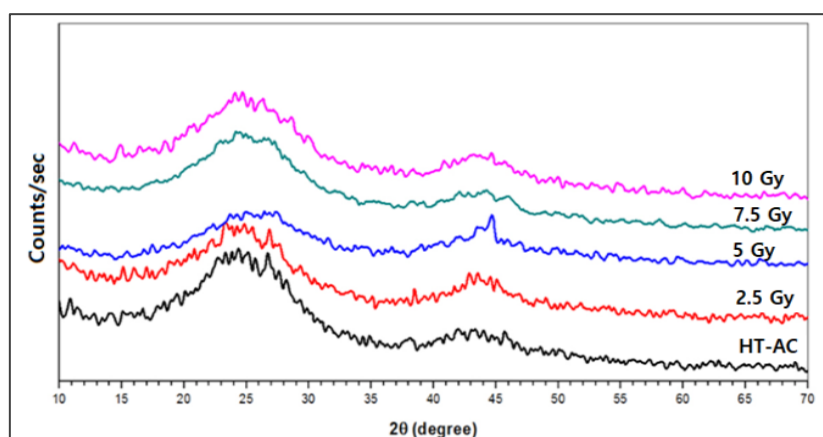

Figure 2: X- ray diffraction analysis of HT-AC and HT-AC species irradiated at various γ-ray doses (2.5-10 Gy).

increase in the pseudo crystallite height (Lc) usually signs higher interlayer spacing than that of the typical graphite, 3.35 Å[29, 30].The up-word decrease in the same peak at higher γ- irradiation of 5-10 Gy, may propose a disordered carbon with turbo stratic structure, This may result from any of the following actions; local faulting in the stacked layers (see Figure 3B), variation in the interspacing, random layers shifting, sluggish presence of carbon debris that are not related to the stacked layer (see Figure 3A&B), and/or layer strain [31].In the literature, the formation of carbon remnants can result from the biomass (cellulose & lignin)degradation by impregnation and pyrolysis in the highly concentrated phosphoric acid (60%), where the pseudo-cellulose parts (short-chain polymeric entities) are preserved in the form of smaller fragments, probably with phosphatic linkage[28, 32]. Thus, the broad diffraction peak with higher elevated nods around the 2θ ≈24° with different d-spacing, may indicate co-presence of residual cellulose, distorted graphene layers, and/or the possible newly developed phosphoric-linked layers[32, 33].

In the same Figure 2, the peak around 2θ ≈43°seemed more diffused with broader and weaker intensities that may imply less developed intra graphitic layers with insignificant change in the lateral sizes of the graphene layers [34, 35]. So far, the obtained XRD result indicated the incomplete destruction of the lingo cellulosic material of the original precursor (HT) after the chemical activation using the 60% concentrated phosphoric acid.

_____

Meanwhile, the ϒ-irradiation maintained the same amorphous nature of the prepared AC in all samples, with notable flattening and reduction in the peak intensities, especially for samples treated with more than 5 Gy doses, may predict more destructive effects encountered in the material at higher gamma dosage of 7.5 and 10 Gy. The obtained XRD result agrees well with literature [36].

3.1.2. SEM and EDX Analysis

The detailed surface morphology of the precursor HT-AC and its irradiated versions (HT-AC$_{2.5-10 \ Gy}$), before and after the pesticide loading, were detected using SEM and EDX micro chemical analysis and presented in Figure 3 and Table2. Figure (3A-E) is showing the micrographs of the product before the Ictafos uptake. The parent HT-AC implied compacted rough surface with two porous domains: one with more or less, uniformly-sized microporosity within the graphene sheets and the other intra-layers grooves and pockets initiated between detached remnants and non-porous ridges, Figure 3A. On applying the gamma rays of 2.5 Gy, some more areas of homogenous porosity were uncovered, and the rough ridges seemed to be quantified into smaller carbon debris, Figure 3B. Moreover, the HT-AC samples exposed to higher γ-doses of 5 Gy indicated carbon with a spongy structure with macro-scale porosity and less uniform texture. This modified material implied surfaces with huge voids of more than 100 μ in size, Figure 3C. The further increase in the applied γ-dose led to a continuous pore-wall thinning up to voids collapsing and a completely tortured structure with much more accumulated debris in the pores and uncontrolled porosity features, Figure 3C-E. The deterioration of the HT-AC structure with increasing gamma doses>2.5 Gy, agrees well with the XRD reduced peaks in Figure 2. In the meantime, the scattering of carbon debris and the mesoporous AC skeleton is indicative of the distracted samples. On the other hand Figure 3F-J is monitoring the same materials but after the Chlorpyrifos adsorption process. As can be seen in Fig. 3F-G, the micrographs specified dense texture with uncovered porosity, accompanied with some adsorption channels and macro porosity.

the development of the mega porosity in samples treated with γ-irradiation at low doses 2.5 - 5 Gy is still presenting a clear porous texture that not clogged with the carbon remnant or particulates, the predictable effect of which is an acceleration in the pollutant sorption processing, Fig.3F-G. On the other hand, samples subjected to higher doses (> 5Gy) showed more hindered surfaces with an inhomogeneous pores distribution and reduced porosity. The said effect could possibly be resulted from the masking effect of the adsorption passages by the collapsed pores, ending with more domains of dense carbon construction, containing burden porosity and cracks, Fig. 3J.

Table 2 presents the EDS chemical microanalysis of the parent HT-AC and its modified (HT-AC$_{2.5-10 \ Gy}$) species. The chemical composition of the prepared materials, whether as-prepared or modified, contained the same elements that are usually contained in the activated carbon, with an average carbon content of around 90%. The Phosphorus (P) is sourced from the chemical activation process by phosphoric acid, whereas iron (Fe) was an original component of the raw material from which the HT-AC was derived Figure 3A-E. Meanwhile, the EDS of the irradiated samples showed many added elements that were not found in the as-prepared HT-AC, such as N, S and Cl. Figure 3F-J and Table 2.

The elements of nitrogen, sulphur, and chlorine are the main constituents of the Ictafos pesticide, and consequently confirming the successful adsorption process[37] and the clear removal of such harmful pollutant onto the surfaces of HT-AC and its γ-irradiated versions. Surprisingly, it was found that the sample HT-AC2.5Gy having the least percentage of the carbon content of 57.3 % adsorbed the highest amounts of the removed pesticide elements (N, S, and Cl), as compared to all other adsorbents with higher carbon content 60-63%. This could be explained in the light of the non-disturbed structure of HT-AC$_{2.5Gy}$which may result in an enlarged surface area and unblocked porous profile, to conveniently supplied an easy passage way for the adsorbed chlorpyrifos. This opinion agrees well with the SEM and XRD results.

Table 2 : Chemical microanalysis of HT-AC and HT-AC (2.5-10 Gy) before and after adsorption process

Adsorbents		Elements (wt %)							
		C	O	Si	Fe	N	P	S	Cl
HT-AC	*Before adsorption*	87.13	7.56	0.49	0.62	-	4.2	-	-
HT-AC 2.5 Gy		83.724	10.9	0.91	0.55	-	4.4	-	-
HT-AC 5 Gy		86.88	7.79	0.5	0.63	-	4.2	-	-
HT-AC 7.5 Gy		83.1	9.01	0.6	1.1	-	4.11	-	-
HT-AC 10 Gy		85.68	8.9	0.45	0.89	-	4.08	-	-
HT-AC	*After adsorption*	59.77	10.2	0.42	0.61	24.62	4.29	0.06	0.08
HT-AC 2.5Gy		57.14	7.3	0.95	0.53	28.95	4.56	0.16	0.14
HT-AC 5Gy		62.98	11.17	0.56	0.60	20.24	4.25	0.11	0.09
HT-AC 7.5Gy		60.6	10.8	0.62	0.97	22.71	4.16	0.08	0.06
HT-AC 10Gy		61.88	13.11	0.47	0.86	19.35	4.2	0.06	0.07

3.1.3. BET

The specific surface area (SE) of all prepared materials was determined by applying NOVA e-Series analyzer using Nitrogen adsorption/desorption isotherms at 77 K. The obtained data are given in Table 3 and Figure 4. Generally, the very high surface area of all samples suggested an efficient chemical and thermal activation processes in converting the raw material to a well-developed activated carbon with huge BET. Results displayed that samples subjected to the low γ-doses doses of 2.5Gy (1702.2 m²/g) and 5Gy (1561.5 m²/g) attained larger SE than those treated at elevated γ-doses of 7.5Gy (1289.4 m²/g) and 10Gy (1368.4 m²/g). Also, it possessed much higher SE than the parent HT-AC (1438.971 m²/g), Figure 4A & Table 3. Compared to the all tested materials, HT-AC$_{2.5Gy}$ retained the highest volume of the micro-scale pores (0.728 cc/gm), and the maximum total pore volume (1.129 cm³/g), which marked this sample as the best adsorbent formed at the optimum preparation conditions. The enlargement of SE of samples at lower γ-doses is evident in the SEM images (Figure 3A-C), whereas, the porosity and structure deformation in the activated carbons treated at 7.5 and 10 Gy doses indicated clear surface disturbance (Figure 3D-E). The probable cause of such effect could be related to the nature and hardness of the Doum husks that could not withstand the high doses of gamma rays and suffered from pore wall thinning to the extent of losing some of its porous identity. The clogging of the pores with the debris resulted from the pores collapsing is an additional reason for the reduction in the carbons specific surface area at higher gamma irradiation doses.

The surface area of the BET was calculated from the isotherm using the Brunauer Emmett Teller (BET) equation[38]. The form of the isotherm of adsorption may provide qualitative details about the adsorption mechanism Figure 4B presents the N$_2$ adsorption isotherms of HT-AC and its irradiated species. It is clear that, all samples isotherms are belonging to type (I), classified by IUPAC [39]. This isotherm type (I) represents the narrow microporous adsorbents having a pore size < ~1 nm, and characterized primarily by monolayer adsorption, where the uptake gradually increases with the pressure and approaches the peak at the saturation pressure.
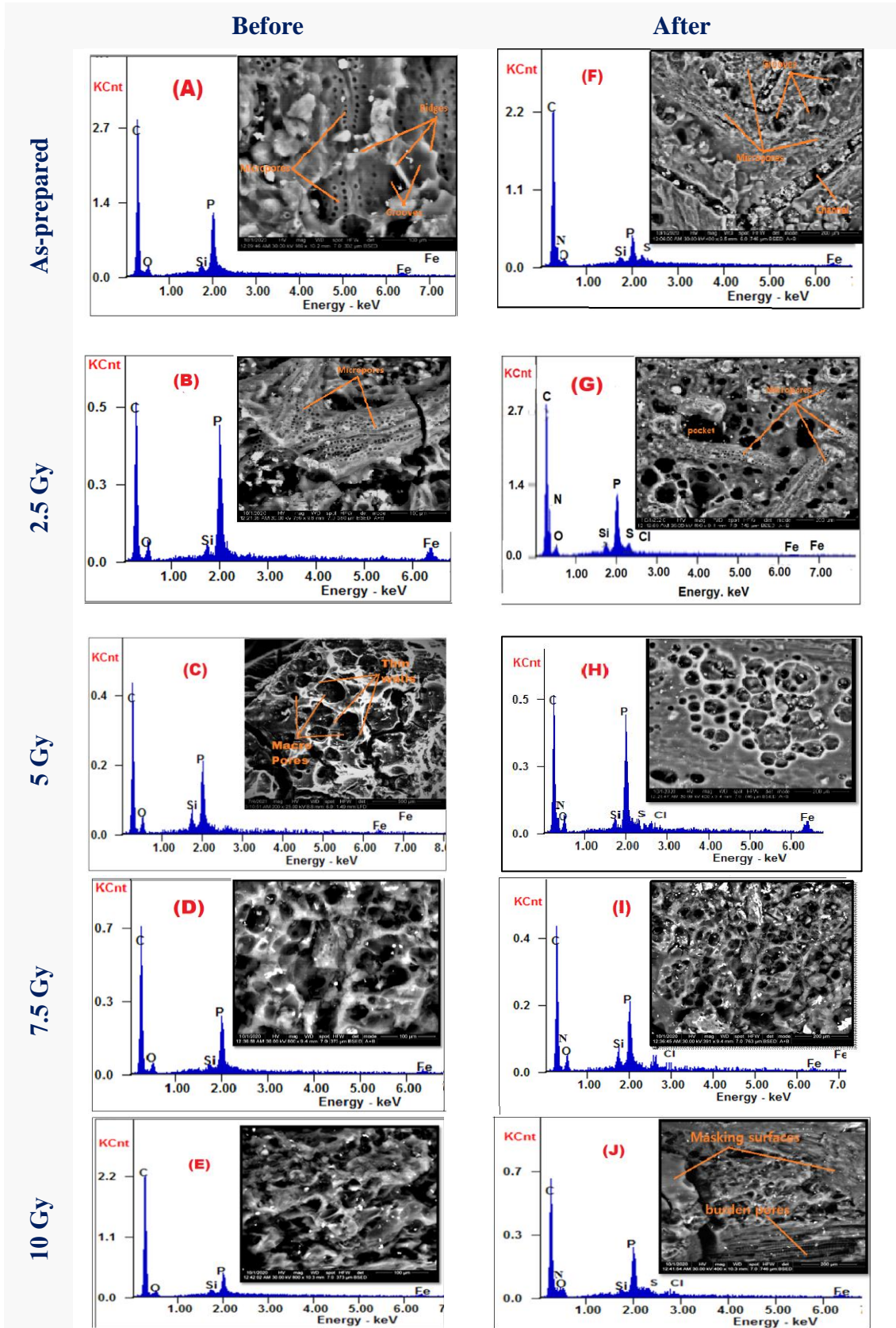
Figure 3: Scanning Electron Microscopy (SEM) images and EDX profiles for the HT-AC samples before (A-E), and after (F-J) the adsorption process of the Chlorpyrifos

Table 3: physical properties of activated carbon HT-AC and HT-AC (2.5-10 Gy)

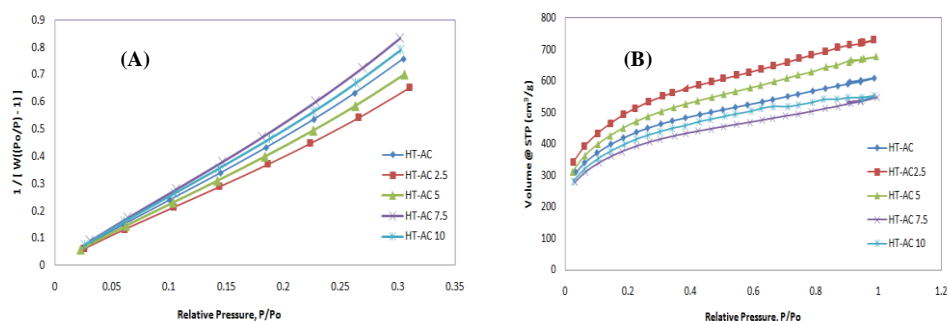| Adsorbents	S_{BET} (m²/g)	V_{Micro} (cc/g)	V_{Meso} (cc/g)	r (nm)	V_{Total} (cm³/g)	Aver $_{Pore Size}$ (nm)
HT-AC	1438.971	0.624	0.288	1.6358	0.9425	1.30997
HT-AC $_{2.5}$	1702.214	0.728	0.356	1.6298	1.129	1.32677
HT-AC $_5$	1561.583	0.669	0.345	1.6198	1.048	1.34186
HT-AC$_{7.5}$	1289.240	0.563	0.256	1.6266	0.8483	1.31604
HT-AC$_{10}$	1368.402	0.589	0.237	1.6275	0.8535	1.24740

Figure 4: The BET surface area of adsorbents (A), the Nitrogen adsorption isotherms for adsorbents HT-AC and HT-AC (2.5-10Gy) (B)
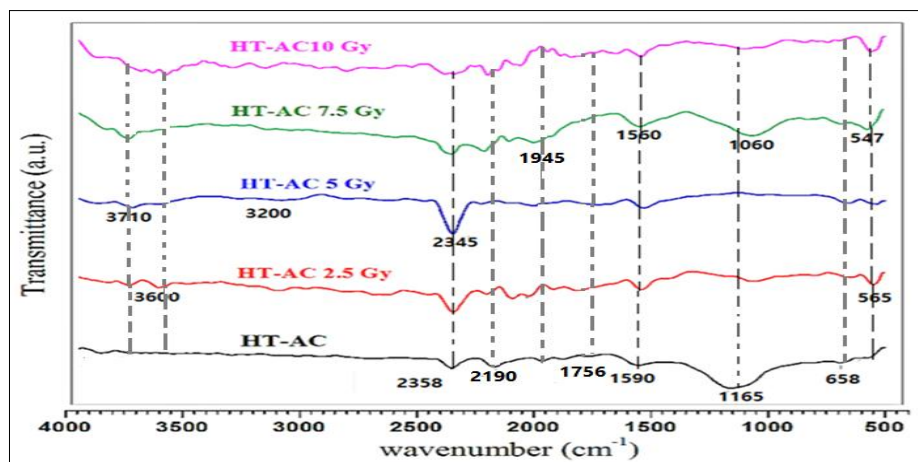
3.1.4. FT-IR analysis

Figure 5A: FT-IR spectra analysis of (HT-AC) and modified activated carbon by gamma rays

The FT-IR spectra of HT-AC and modified activated carbon by gamma raysHT-AC (2.5-10 Gy) can be seen in
Figure 5A, and FT-IR spectra for raw HT-AC and HT-AC (2.5-5 Gy)before and after adsorption of CPF pesticide are shown in Figure 5B. For the precursor sample (HT-AC), the main FT-IR bands are presented in Table 4.

The weak transmittance bands around 3700 and 2700 cm^{-1} may be ascribed to isolated O–H[40], and the asymmetrical aliphatic C-H for methyl and methylene groups [41], respectively. The strong band around 2358 cm^{-1} can be attributed to C≡C stretching vibrations in alkyne groups [42], it is strongly developed in the samples treated with gamma doses of up to 5Gy, but it decreases on increasing the dosage up to 10 Gy. This may limit the positive effect of gamma rays on the carbon structure up to 5Gy, after which the band seemed smaller with shallow appearance. The previous effect agrees well with the

_____

results of XRD and SEM sections of this paper, sections 3.1.1 & 3,1,2. The different small bands in the areas of 2200-1950 cm^{-1} are due to the C-O bond stretching, and the one at around 1756 cm^{-1} is a characteristic band of the C=O stretching vibrations of ketones, aldehydes, lactones or carboxyl groups[43]. The spectra of all prepared activated carbons species also reveal a clear band around 1650-1560 cm^{-1} due to C-C vibrations of the aromatic rings. The broad band at 1000–1300 cm^{-1} with epics at 1165 cm^{-1} is most commonly related to oxidized carbons and has been assigned to C–O stretching in acids, alcohols, phenols, ethers or esters groups[44].However, it is also characteristic to phosphorous containing functionalities, so the peak at 1150-1200 cm^{-1}, may also reveal hydrogen-bonded P=O and O–C stretching vibration in P–O–C (aromatic) and P–O in acidic phosphate esters [45]. It has been mentioned that, the increment in the IR

spectral intensities for the stretching vibrations of the O-H (hydroxyl), C=O (carboxylic) and C-O (phenol) groups can present the formation of more functional groups of oxygen on the phosphorized activated carbon[46]. The process of chemical activation using phosphoric acid can be considered as that occur during the coal liquification by Lewis acids, i.e. reactions of acid-catalysis cracking. In such method, the linkages between cyclic structures (etheric, methylenic, and thioetheric) in the carbon can be subjected to rupture due to the acid catalysis via ionic mechanisms, resulted in bond breaking after protonation[47]. Other bands below 950 cm^{-1} are caused by out-of-plane deformation of the vibrations of C-H groups in the aromatic structures[42]. The very shallow shoulder of the band around 3400cm^{-1} which is characteristic to the O-H groups may indicate very little adsorbed water in the AC structure.
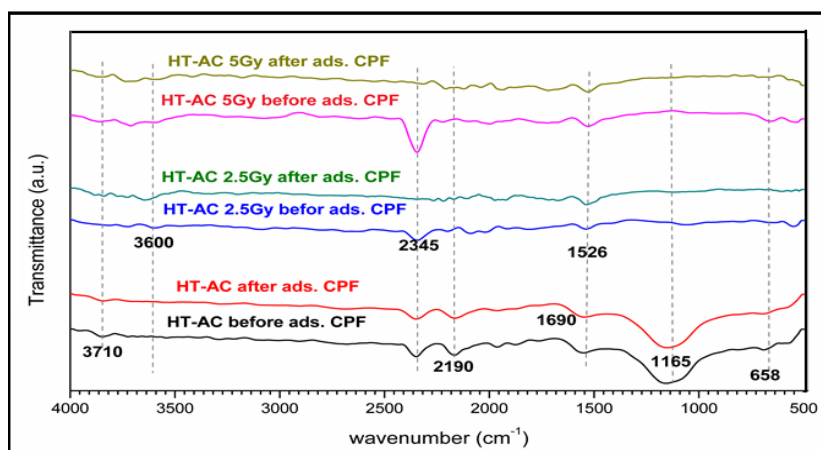

Figure 5B: FT-IR spectra for raw HT-AC and HT-AC (2.5-5 Gy) before and after adsorption of CPF pesticide

As can be seen from Figure 5B, the IR spectra for the raw HT-AC sample indicated the preservation of the main positions and strengths for the structural groups after CPF adsorption application. Whereas, 2.5 and 5Gy irradiated carbons displayed shallower bands, when compared to their irradiated versions before CPF sorption, especially those at 2345cm^{-1} (which assigned to C≡C stretching vibrations in alkyne groups) and that one at 1165 cm^{-1}(related to the oxidized carbonsC–O stretching in acids, alcohols, phenols, ethers or esters groups, hydrogen-bonded P=O and O–C stretching vibration

in P–O–C (aromatic) and P–O in acidic phosphate esters). During the adsorption process, the former band (2345 cm^{-1}), assigned to C≡C stretching vibrations in alkyne groups, may suffer turbostratic structure with disordered carbon resulted from localized fracturing and/or random shifting in the stacked layers, interspacing variation, presence of carbon debris that are not related to the stacked layer, and/or layer strain[31]. The tensions in the layers may proceed to structural-failure and air-washable fragmentation, especially under the flow of air, applied during CPF adsorption.

_____

Table 4: The main FT-IR bands for the as-prepared HT-AC and its γ-irradiated modified samples

Bands (cm⁻¹)	Chemical group	References
3710	Stretching vibration of isolated -OH group	[40]
2700	Carboxyl group	[41]
2250-2400	C≡C stretching vibration, carbon-carbon triple bone of alkynes	[42]
2200-1950	C-O bond stretching	[43]
1650-1560	C-C vibrations in aromatic rings	[44]
1150-1200	Hydrogen- bonded P=O, O-C stretching in P-O-C (aromatic) & P-O in acidic phosphate esters	[45]
<950	Out of plane-C-H bending	[48]

3.1.5. Raman spectroscopy

The ratio of the obtained intensities of the D and G bands reflects the ordering and disordering of the carbon structure Figure 6 displays the Raman spectra of the as-synthesized activated carbon (HT-AC) and its modified forms after irradiation by different gamma doses, HT-AC (2.5-10 Gy), while, while Table 5 presents the calculated ID/IG values for the samples. The spectra identified two characteristic bands; G- at 1593cm⁻¹ signifies the in-plane vibration of SP^2 bonded carbon atoms in the rings and chains (ordered), and D- at 1359 cm⁻¹ marks the structural defects due to the sp2 vibrations out of plane or in rings (disordered), respectively[49].The ratio of integrated intensities D and G bands (ID / IG) is used to ascribe the number of polycrystalline carbon material disorders.[50]. In comparison, the G band maximum position of HT-AC$_{2.5Gy}$ was shifted from 1593 cm⁻¹ (original HT-AC) to a lower value of 1587 cm⁻¹, and its calculated ID/IG ratio was decreased from 0.92 in the parent AC carbon to 0.861. The previous finding can indicate a material with partial transformation to more ordering structure or from amorphous to a more graphitic lattice[51, 52]. This previous conclusion marks the γ-dosage of 2.5 Gy to be the most appropriate for the HT-AC modification. This result was ascertained and complied with the other findings from XRD, SEM, and FT-IR results. Generally, other γ-irradiated carbons at 5 and 7.5 Gy doses implied G-band maxima shifting to a higher value of 1600.5, and 1594.5cm⁻¹ than the G band of the as-prepared HT-AC, meanwhile their corresponding ID/IG decreased to 0.662, and 0.739 than that of the original AC band value, 0.924.

The reduction in the ID/IG may indicate more graphitic material with oriented and planner structure. However, the modification via oxygenation in the lattice of carbon can occur during γ-irradiation, a replacement between environmental oxygen and

graphene carbon can result in the elevating of the G-band maxima to a higher position[53].

In the same context and in agreement with the FTIR, the chemical activation of the HT-AC with phosphoric acid (H_3PO_4) aqueous solution (conc.60 %) led to the formation of more functional groups of oxygen on the phosphorized activated carbon. It has been mentioned that, the oxidized substances are more susceptible and sensitive to γ-irradiation[54]. The HT-AC $_{10Gy}$ material, although implied the highest G-band shifting (1608cm⁻¹), it implied the highest ID/IG value (1.10) of all samples. This can indicate that the highest γ-dosage of 10 Gy induced the maximum graphene disordering structure. The same result was congruent with the XRD, FTIR, and SEM results.

Table 5 Calculated ID/IG for all samples

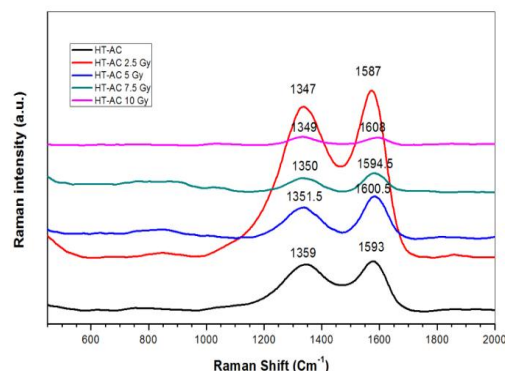| Sample	ID/IG
HT-AC	0.924
HT-AC $_{2.5 Gy}$	0.861
HT-AC $_{5 Gy}$	0.662
HT-AC $_{7.5 Gy}$	0.739
HT-AC $_{10 Gy}$	1.10

Figure 6: Raman microscopy analysis of (HT-AC) and modified activated carbon by gamma rays

_____

_____

3.2. Effect of Gamma irradiation onto adsorption efficiency.

The effect of γ-rays on the efficiency of the Ictafos adsorption process has been studied under fixed (optimum) experimental parameters including; initial concentration of 50 ppm, flow rate 0.5 L.m^{-1}, material 0.75 g, and temperature of 26 $^{\circ}$C. Figure 7A&C shows the sorption capacity of each AC species, whereas, Figure 7B&D represents the efficiency of their removal capability in percentages. Obtained results showed a remarkable increase in the pesticide uptake capacity for the AC irradiated at lower γ-doses up to 5 Gy, with the highest performance for the HT-AC $_{2.5}$. The corresponding effluent elimination amounts were; 400,480, 450, 333 and 360 mg. g^{-1}, for the parent HT-AC, HT-AC 2.5,5, 7.5 and 10 Gy, respectively. Figure 7B&D implies the removal efficiency (%) for all prepared AC substances, where the decrease in efficacy was noticed in materials treated with γ-dosage larger than 2.5 Gy (Figure 7B, D). Therefore, HT-AC subjected to the lowest γ-irradiation of 2.5 Gy was the most convenient adsorbent for the air polluted with Chlorpyrifos pesticide. This may be attributed to its relevant highest surface area among all other prepared adsorbents.
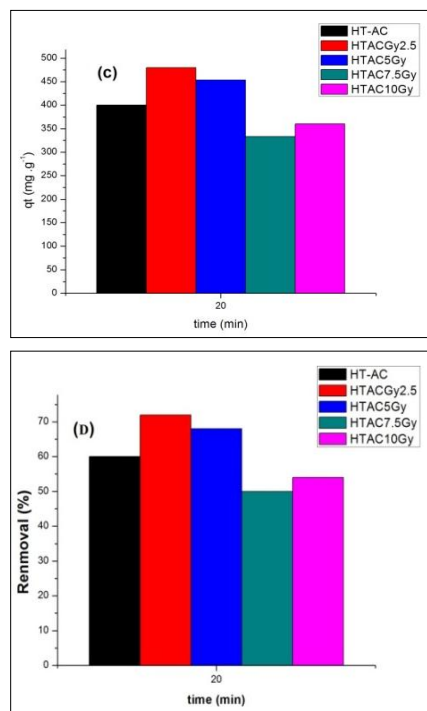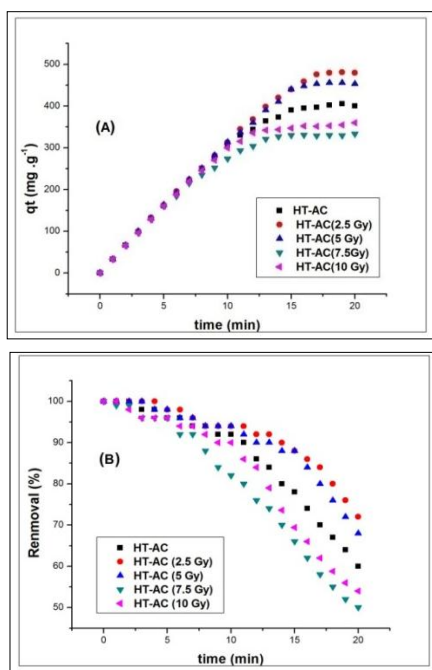

Figure 7: Effect of Gamma irradiation onto adsorption capacity and adsorption efficiency

3.2.1. Mechanism of Gamma radiation effect on surface morphology of activated carbon

In the radiation process, heat is found to be transferred as electromagnetic energy without the need for a medium. In most probable mechanism for the gamma irradiation effect on morphology of AC can be traced as follows; the activated carbon absorb all incident radiation (energy transfer), then the absorbed energy was found to cause some chemical and physical changes on the activated carbon surface[55]. The radiation effect on the surface area depends mainly on the dose of gamma irradiated and the nature of adsorbent material as shown in Figure 8. When a material is irradiated with ions or electrons, atoms can be displaced from their lattice sites due to elastic collisions involving the incident projectiles. As a result, the vacancies produced by the displacement damage can introduce defect states within the band gap of active materials. These defect states deteriorate the performance of the materials. In addition to the displacement damage caused by energetic recoil electrons, the holes produced during the compton scattering can make change in porosity, surface area , and can also form oxides and interface charge traps[56].This mechanism explanation agrees

with the results of EDX, where, an increase in the oxygen contents was observed with gamma irradiation (Table 2). The SEM results also supports this mechanism and the micrographs of Figure 3 implied some morphological changes in the irradiated HT-AC samples and showed the evolution of pores and cracks on the irradiated surfaces. It has been suggested that in the irradiated samples, oxygen moves into an interstitial site and creates oxygen-vacancy complex and modified stoichiometry may result in the near surface region[57].Obviously, the development of the mega porosity in samples treated with γ-irradiation at low doses 2.5 - 5 Gy is still presenting a clear porous texture[58]. On the other hand, samples subjected to higher γ-doses (> 5Gy) showed more hindered surfaces with an inhomogeneous pores distribution, cracks and reduced porosity, this outcome was also achieved by BET analysis Table3. The deterioration of the HT-AC structure with increasing gamma doses >2.5 Gy agrees well with the XRD reduced peaks in Figure 2. In the meantime, the scattering of carbon debris and the mesoporous AC skeleton is indicative of the distracted samples. From all mentioned evidences, the gamma irradiation of the materials changes the physical and chemical properties of the samples[59].
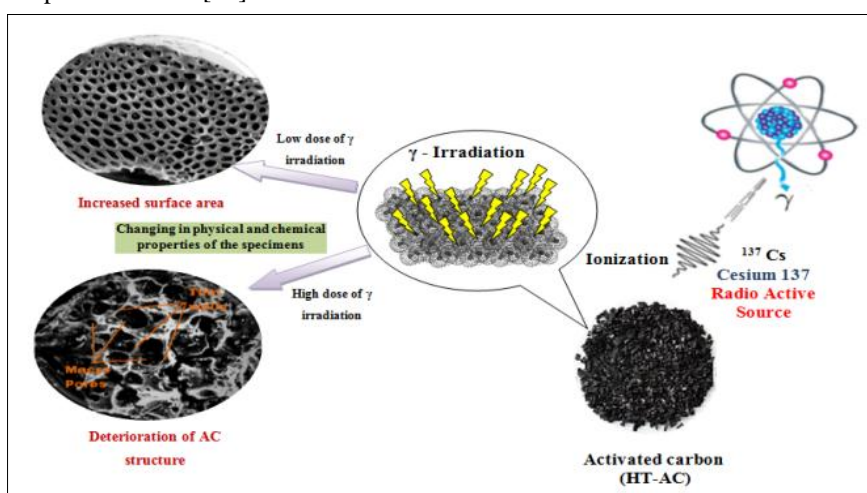

Figure 8: Schematic diagram for mechanism of gamma irradiation effect on morphology of AC

3.3. Effect of adsorbent dosage

This study was applied to the as-prepared carbon, HT-AC, compared with two γ-irradiated adsorbents that were structurally and physically reflecting the most appropriate properties from XRD, FT-IR, SEM, BET, etc., samples 2.5 and 5 Gy. The quantity of the used adsorbent has a great influence on the pollutant elimination process and extremely controls the hazardous material. The AC doses in the range of 0.25 to 1.0 g were applied under the optimum experimental conditions of $26°C$ temperature, 0.5 L min^{-1} rate of gas flow, and 50 ppm for the concentration of chlorpyrifos in gas phase inlet. The obtained results are shown in Figure 9A-F.

Based on the time scale, from 0–20 min, the pesticide uptake capacity was evaluated to establish the optimum sorption time. The results revealed that there was a decrease in the capacity and initial rate of adsorption of the pesticide with increasing the activated carbon dosage, Figure 9A, C and E. This behaviour is quite normal and its possible explanation is the high availability of active centers on the surface of excess adsorbent which consumed the whole pesticide elements onto some of its vast surface area sites, leaving much more carbon vicinities unsaturated [60]. Accordingly, Figure 9B, D and F indicates the direct relationship between the increase in the AC dose and the rise up of the adsorption efficiency. The increase in the quantity of sorbent magnifies the active centres required for chlorpyrifos uptake, which in turn fastened the adsorbents removal and increase its efficiency per unit of weight[61, 62].
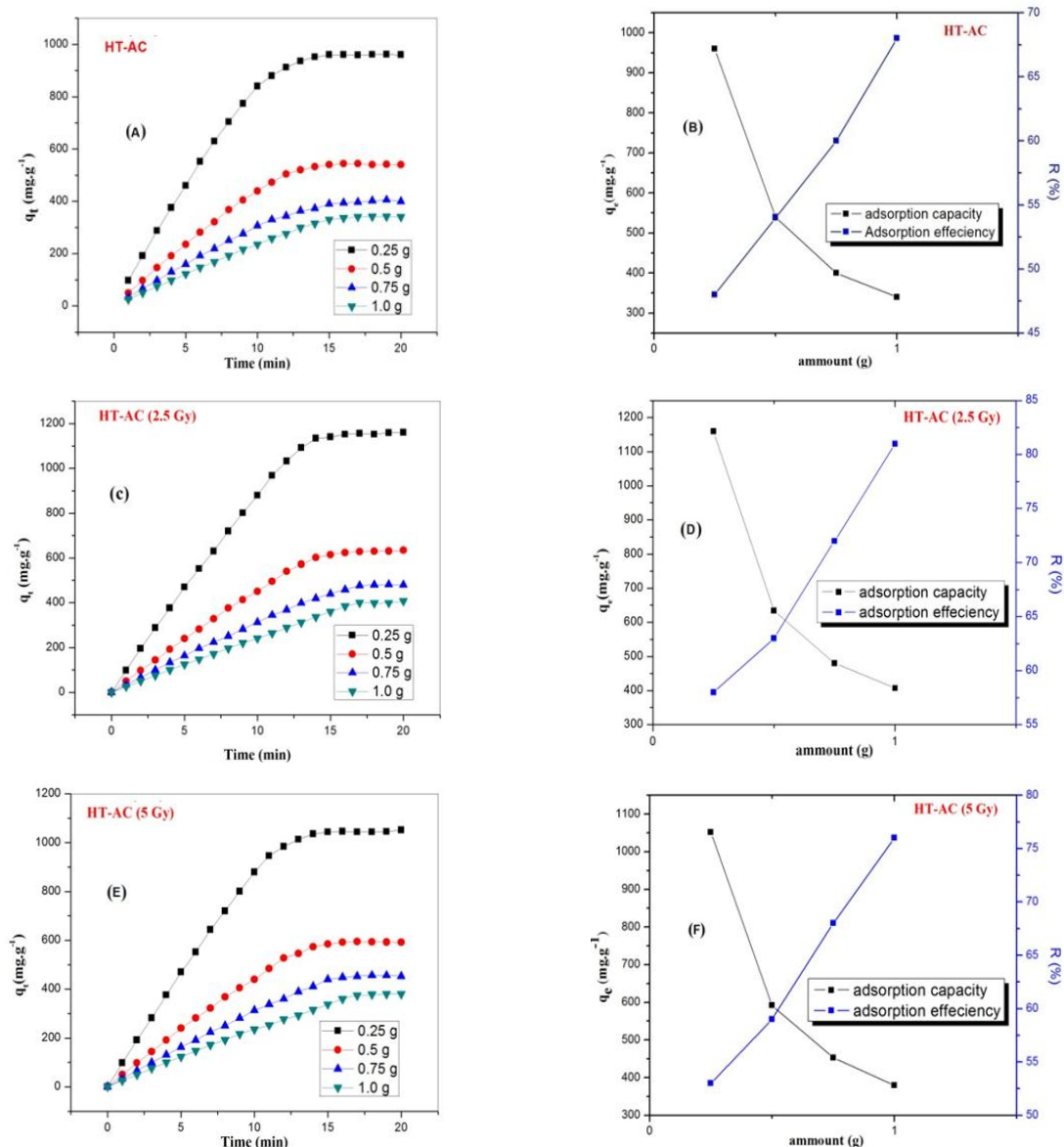
_____

Figure 9: Effect of the amount (g) of HT-AC and HT-AC (2.5 and 5 Gy) on the adsorption of Chlorpyrifos with time (min.) (a, c and e). The adsorption capacity (qe mg.g-1) and the adsorption efficiency (R%) (b, d and f) of the adsorbed Chlorpyrifos.

3.4. Effect of gas flow rate (FR)

The effect of gas flow rate on the adsorption capacity and the removal percentages of the Ictafos were investigated in the range of 0.3 to 0.6 $L.min^{-1}$ and represented in Figure 10A-F. As can be seen, there is a decrease in the adsorbate uptake at different FRs as the process reached the equilibrium. The adsorbed amounts of pesticide by all samples showed no significant effect by increasing the FR, except for the materials irradiated at 2.5 and 5 Gy which were

slightly adsorbed relatively higher amounts of the pesticide pollutant at higher FR, Figure 10C&E. Seemingly, the upward rise in the flow rate resulted in a relevant elevation in the adsorption capacity but with a deterioration in the process efficiency with time, Figure 10B, D and F. Hence, the least FR (0.3 L min^{-1}) can be considered as the optimum due to its accompanied maximum efficacy with HT-$AC_{2.5Gy}$ and HT-AC_{5Gy} materials [21]
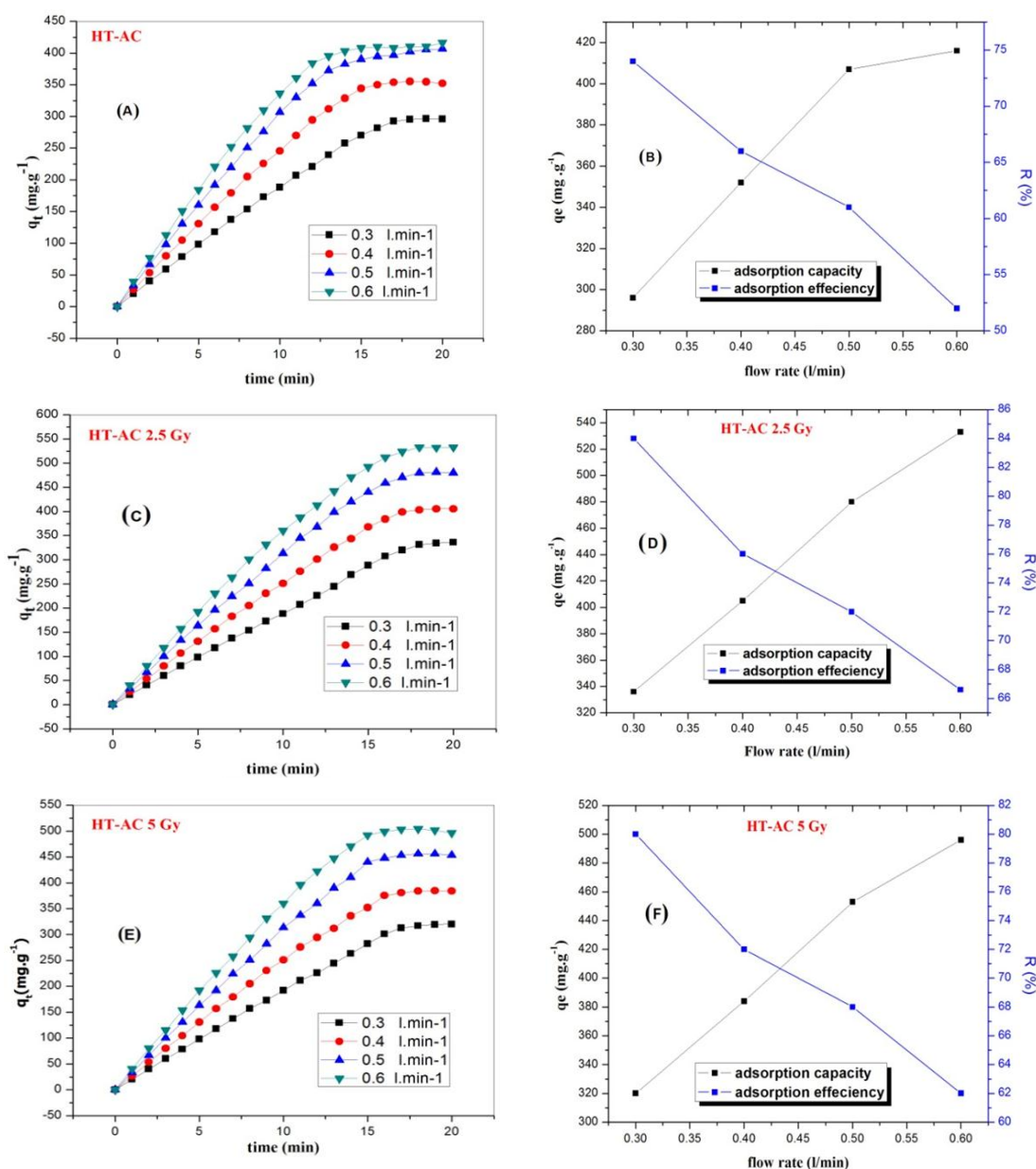
_____

Figure 10: Effect of gas flow rate on the adsorption of Chlorpyrifos onto HT-AC and HT-AC (2.5 and 5 Gy)

3.5 Effect of pollutant concentration

The effect of Chlorpyrifos concentration in the range of 40-70 ppm (in gas phase) on the adsorption capacity and efficacy of the tested AC species was investigated at different gas-feeds and constant conditions of 0.5 L min^{-1} flow rate, 26 $^\circ$C and definite dose of 0.75g for each AC species.

The results are given in Fig11 A-F. The attained data indicated the on-going decrease in the AC uptake efficiency on increasing the initial gas concentration[63]. Such behaviour is normally seen in

the light of the rapid saturation of the samples due to the fastened interaction between the excessive added pollutant molecules and a constant surface area of the adsorbent, the resultant is a shorter exhausting time and an accelerated sorption process with an early equilibrium state [64].

It should be noted that, the adsorption efficiency of all samples was superior with the least value of 96% for the parent HT-AC, and the highest of 100% for the treated substances with 2.5 gamma dosage, which

prove the high performance of the locally prepared AC, as-prepared and modified. However, the lab outcomes governing the adsorption process marked an advantageous effect for the irradiated HT- AC species, possibly due to the enlarged surface area for HT-AC 2.5 and 5 Gy versions. It is a fact that, lab testing showed higher rate of pesticide sorption onto the gamma-modified materials than that of HT-AC one, and confirmed a notable increase in the chlorpyrifos uptake on increasing the treatment concentration in the range of 50 to 70 ppm.
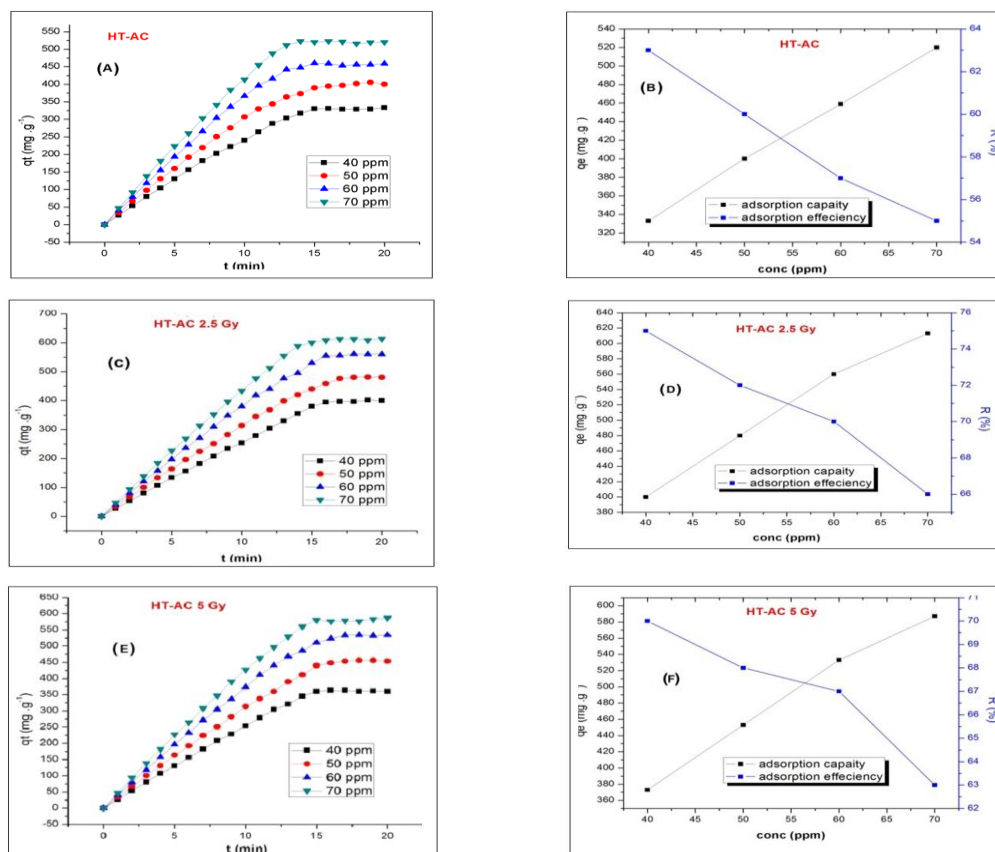

Figure 11: Effect of different concentrations of chlorpyrifos adsorbed onto HT-AC and HT-AC 2.5 and 5 Gy

3.6. Effect of temperature

In the physical sorption processing, molecules of pollutants are adsorbed inside the micro and mesopores of the AC structure, providing an easy passage for the transportation of adsorbate through the substance. Experimentally and at fixed conditions of 50 ppm pollutant concentration and 0.5 L.min-1 FR, there was a notable decrease in the Ictafos removal percentage and reduction in the uptake capacity of the tested samples on increasing the testing temperature from 291 K to 315 K, Figure 12. This process behaviour indicated a physical gas-sorption process of exothermic nature[65], wherein,

the measured efficiencies were retreated on elevating the experimental temperature from 291 K to 315 K; the obtained values were lowered from61 to 46% for HT-AC, 74 to 60% for HT-AC2.5 Gy, and 70 to 56 % for HT-AC5Gy . 3.7. Kinetic modeling

The dynamics of the Chlorpyrifos adsorption reaction process in terms of the order and the rate constant can be estimated using the kinetic data. To study the controlling mechanism like rate controlling step, diffusion control, chemical reaction and mass transfer, the adsorption onto the HT-AC, HT-AC 2.5 and HT-AC 5 Gy were analyzed using pseudo-first-order [66] expressed by Eq. 4,
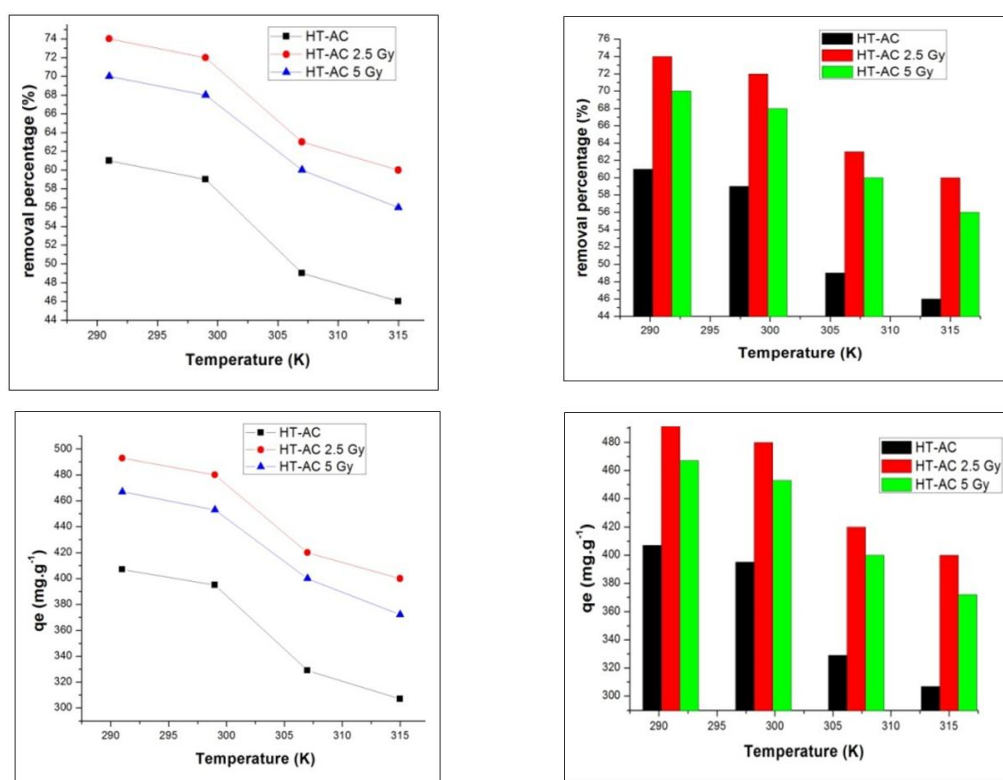
Figure 12: Effect of different temperatures on the adsorption capacity and removal percentage of the Chlorpyrifos adsorbed onto HT-AC and HT-AC (2.5 and 5 Gy).

pseudo-second-order [67] expressed by Eq. 5&6 and intra-particle diffusion [68] by Eq. 7) kinetic models.

$$\ln(q_e - q_t) = \ln q_{e,1} - k_1 t \text{-----------------------}$$
----(4)

$$\frac{t}{qt} = \frac{1}{k_2 q_{e,2}^2} + \frac{1}{q_{e,2}} t \text{-----------------------------------}$$
(5)

$$h = k_2 q_{e,2}^2 \text{---}$$
(6)

$$q_t = K_i t^{0.5} + C \text{-----------------------------------}$$
(7)

Where q_e and q_t are the volatile organic compounds (VOCs) amount adsorbed per unit mass of the sorbent at equilibrium and at a time t, respectively (mg/g).

k_1 and k_2 are the pseudo-first - order (min^{-1}) and pseudo-second-order (gm mmol^{-1}min^{-1}) sorption constants, respectively.

The values of rate constant (k_1) and equilibrium capacity ($q_{e,1,\text{cal}}$) can be gained from the slope and intercept, respectively by plotting log ($q_e - q_t$) against

time, Figure 13A.The values of k_2 can be determined from the plot of t/q versus t, Figure 13B. Furthermore, the initial rate of adsorption (h) (mg/g min) also calculated. k_i is the intra-particle diffusion rate constant (mg/g min$^{1/2}$) and C (mg/g) is the film thickness. Table 6 provides the corresponding kinetic coefficients obtained for different models. By comparing the correlation coefficients R^2 obtained for each model, the pseudo-first-order is more suitable in describing the Chlorpyrifos adsorption reaction for all tested AC samples. The initial adsorption rate (h) for pesticide gas invading onto the surfaces of samples, increased with increasing the pesticide concentration from 40 to 70 ppm. This starting period of adsorption presented the highest rate of pollutant uptake in the whole process.

Figure 13C is shows the intra-particle diffusion model (IPD). The large intercept value is marking a large contribution of the surface adsorption, which may suggest the IPD to be the main controlling step in the pollutant adsorption processing through AC materials. To do so, the linear part of that intercept must pass through the origin of the plotted relation

_____

between q_t and $t_{1/2}$, which is not the case here, Figure 13C. Based on this results, IPD may be seen as just a rate-control factor and not the sole one. Therefore, the external surface of the samples is highly considered as the key factor in the rate-

controlling step. The plot deviation from the linearity indicates that, the rate-limiting step should be regulated by the boundary layer diffusion[69].
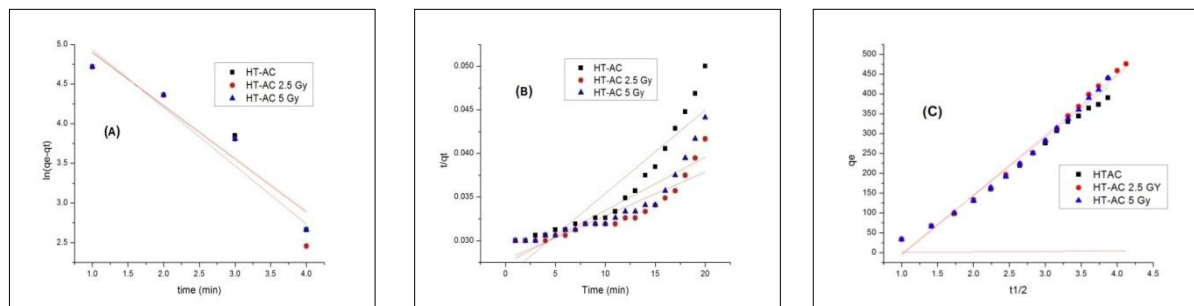

Figure 13: Kinetic models for HT-AC, HT-AC $_{2.5Gy}$ and HT-AC $_{5Gy}$ at concentration 50 ppm (a) Pseudo first order, (b) Pseudo second order and (c) Intra-particle diffusion model

Table 6: Kinetic parameters of the Chlorpyrifos pesticide adsorption, in its gaseous state onto HT-AC, HT-AC$_{2.5Gy}$ and HT-AC$_{5Gy}$

Adsorbent	Conc. (ppm)	Pseudo first-order model			Pseudo second-order model				Intraparticle diffusion model		
		$q_{e,1,cal}$ (mg/g)	K_1 (min⁻¹)	R^2	$q_{e,2,cal}$ (mg/g)	K_2 (g/mg min)	h (mg/g min)	R^2	K_{int} mg/g min⁻⁰·⁵	C (mg/g)	R^2
HT-AC	40	5.249	0.580	0.926	925.925	0.000036	30.769	0.813	111.20	107.17	0.990
	50	5.564	0.666	0.883	1046.20	0.000035	38.684	0.851	133.50	124.52	0.991
	60	5.413	0.693	0.930	1104.43	0.000039	47.915	0.812	162.66	154.23	0.988
	70	6.143	1.321	0.827	1217.87	0.000038	55.991	0.820	183.93	171.17	0.985
HT-AC 2.5 Gy	40	5.340	0.634	0.893	2042.65	0.000007	28.506	0.665	128.39	139.66	0.977
	50	5.667	0.733	0.865	1991.21	0.000009	35.932	0.809	151.39	158.09	0.986
	60	5.460	0.733	0.926	2139.44	0.000010	43.878	0.773	180.67	186.36	0.986
	70	6.135	1.321	0.838	2018.37	0.000013	52.110	0.758	206.05	210.42	0.983
HT-AC 5 Gy	40	5.340	0.634	0.893	1402.51	0.000015	29.429	0.736	122.06	127.12	0.981
	50	5.564	0.671	0.898	1638.26	0.000014	36.549	0.795	146.39	148.66	0.984
	60	5.406	0.693	0.941	1780.52	0.000014	44.503	0.798	173.97	174.45	0.989
	70	6.135	1.321	0.838	1689.49	0.000019	52.910	0.813	195.70	192.09	0.988

3.8. Thermodynamic parameters

Experiments were conducted at different temperatures of 291, 299, 307, and 315 K, to calculate thermodynamic parameters for pesticide sorption on the surface of the selected samples. Based on the Van't Hoff equations (8), enthalpy (ΔH) and entropy (ΔS) were determined[70]. Also, the estimated activation energy (Ea) and sticking probability (S*) were detected from a modified Arrhenius type equation (10) [71], whereas, Gibbs

free energy change (ΔG) was calculated from equation (13). All data are recorded in Table 7

Van't Hoff equation:

$$\ln K_d = \frac{\Delta S^o}{R} - \frac{\Delta H^o}{RT} \text{-----------------------------------(8)}$$

$$K_d = q_e/C_e \text{---(9)}$$

Where R is the universal gas constant (8.314 J mol⁻¹ K⁻¹), T is the absolute temperature(K), qe(mg/g) is the amount of the pesticide adsorbed at equilibrium,

and C_e (mg/l) is the equilibrium concentration of the pesticide in gas phase. The ΔH and ΔS values were gained from the slope $\left(\frac{-\Delta H}{R}\right)$ and intercept $\left(\frac{\Delta S}{R}\right)$ respectively, of the plot of $\ln K_d$ vs. $\frac{1}{T}$ as shown in Figure14A.

Arrhenius equation:

$$S^* = (1 - \theta) \exp\left(-\frac{E_a}{RT}\right) \text{-----------------------}(10)$$

$$\theta = 1 - \frac{C_e}{C_0} \text{-----------------------------------}(11)$$

$$\ln\frac{C_e}{C_0} = \ln S^* + \frac{E_a}{RT} \text{-----------------------------}(12)$$

Where C_o is the initial concentration and C_e is the concentration of Chlorpyrifos pesticide at equilibrium, S^* is the probability of sticking and it is a function of the adsorbent system under consideration and depends on the temperature of the system. The values of E_a and S^* were gained from

the slope $\left(\frac{E_a}{R}\right)$ and intercept $\ln S^*$, respectively, of the plot of $\ln\frac{C_e}{C_0}$ vs. $\frac{1}{T}$ shown in (Figure14B), where

$$ln\ (1\text{-}\theta) = ln\ \frac{C_e}{C_0}.$$

Gibbs free energy equation:

$$\Delta G^o = \Delta H^o - T\Delta S^o \text{--------------------------} (13)$$

In Table 7, the negative sign of enthalpy (ΔH) for the chlorpyrifos adsorption, indicates the exothermic nature of the reaction (ΔH°< 20 kJ mol⁻¹), whereas the ΔS° negative value signified the decrease in the number of species at the solid-gas interface. In the same time, the positive ΔG values of the pesticide uptake on HT-AC, HT-AC 2.5 and HT-AC 5 Gy powders, suggested a non-thermodynamically feasible adsorption and that, the process is non-spontaneous on rising up of the temperature in the range of 18 to 42 °C.

Table 7: Thermodynamic parameters for adsorption of the chlorpyrifos pesticide

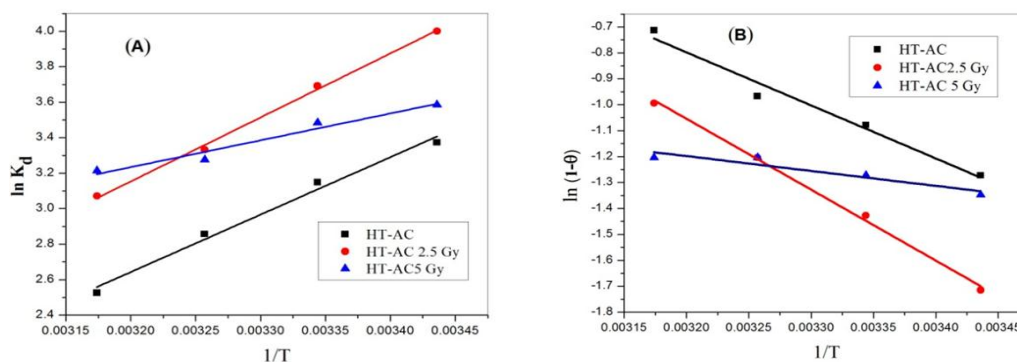| Adsorbent	Temp. (K)	ΔG (kJ/mol)	ΔS (J/mol k)	ΔH (KJ/mol)	S*	Ea (KJ/mol)
HT-AC	291	18.64	-64.16	-26.916	314.10	17.012
	299	19.15				
	307	19.73				
	315	20.18				
HT-AC 2.5 Gy	291	20.27	-69.78	-30.002	2203.34	22.74
	299	20.83				
	307	21.46				
	315	21.95				
HT-AC 5 Gy	291	3.878	-13.37	-12.581	259.30	15.49
	299	3.985				
	307	4.106				
	315	4.199				

Figure14: Thermodynamics models for HT-AC and HT-AC 2.5 and 5 Gy, (A) Van't Hoff and (B) Arrhenius

The effect of temperature on the sticking probability (S*) was evaluated by measuring the surface coverage in the previous temperature range. In Table 7, the sticking probability of Ictafos in the gas phase for HT-AC was found to be very low since all calculated S* values were larger than 1. Generally speaking, the extent of (Ea) can give an idea about the nature of the adsorption process, values less than 40 kJ mol^{-1} signs a physical process features, and those ones of more than 40 kJ mol−1 suggests a chemical adsorption [72]. Accordingly, the process controlling the adsorption of the ictafos pesticide for the tested samples was a physical one, sinceall calculated Ea (kJ/mol) values were less than 40 kJ mol^{-1}. The physical interaction between the adsorbate and adsorbent can probably resulted from hydrogen bonding, Vander Waals force, or electrostatic force. Figure14 represent the thermodynamics models of AC.

3.9. Adsorption studies of isotherm

Besides the experimental consequences, the linearized types of the equations of Langmuir[73] and Freundlich[74] models are widely applied to describe the isotherms of adsorption, equations 14&15. Experimental and theoretical isotherms for the HT-AC and HT-AC (2.5 and 5Gy) confirmed the

elevation of adsorption on increasing the Ictafos concentration in the range of 40-70 ppm for all samples.

Freundlich isotherm: $\ln q_e = \ln K_f + \frac{1}{n}\ln C_e$ ---- (14)

Langmuir isotherm: $\frac{C_e}{q_e} = \frac{1}{bQ_{max}} + \frac{C_e}{Q_{max}}$ ---------- (15)

$R_L = \frac{1}{1+bC_0}$ --- (16)

Where K_f (mg g^{-1}) and n are isothermic constants, indicating the adsorption capacity and intensity, respectively. Freundlich plots of ($\ln qe$ $vs.\ln C_e$) is given for the adsorption of chlorpyrifos onto AC materials at different concentrations. Where $C_e$is the equilibrium concentration of adsorbate (mg L^{-1}),q_e is the amount of gas sorbate at equilibrium (mmol g^{-1}), b is a constant of the Langmuir adsorption (L mmol^{-1}) and Q_{max} is the theoretical maximum adsorption capacity (mg g^{-1}) .

Langmuir plots$\left(\frac{C_e}{q_e}\ vs.C_e\right)$ for adsorption of chlorpyrifos onto the tested AC materials at different concentrations. A dimensionless constant (R_L), commonly known as a separation factor or equilibrium parameter, may be used for the Langmuir isotherm model to describe the adsorption favourability on the adsorbent surface, and C$_0$ is the initial gas concentration.

Table 8: Freundlich and Langmuir modeling for adsorption of the chlorpyrifos pesticide

Adsorbent	Freundlich			Langmuir							
	1/n	K_f (mg/g)	R^2	Q_{max} (mg/g)	K_L (L/mg)	R_L					R^2
						40 ppm	50 ppm	60 ppm	70 ppm		
HT-AC	0.534	4.358	0.998	869.565	0.041	0.381	0.330	0.291	0.260		0.992
HT-AC 2.5 Gy	0.490	4.863	0.966	970.874	0.070	0.263	0.223	0.193	0.170		0.985
HT-AC 5 Gy	0.609	4.389	0.961	2924.096	0.011	0.688	0.639	0.596	0.558		0.665

Table 8 shows the isothermal models, where the correlation coefficients (R^2) for the Freundlich equation was excellently fitted to the experimental data for both adsorbing HT-AC and HT-AC 5 Gy samples, indicating a multilayer adsorption mechanism for heterogeneous surface with no-uniformity, where the active sites are distributed exponentially. In general, the adsorbate molecules and adsorbent used to have strong interaction when the reciprocal of Freundlich constant is larger than 1. Accordingly, the n parameter derived from the

Freundlich model in the current work, has often been greater than 1, confirming the physical adsorption of the pesticide on activated carbon surfaces. Also, the values of l/n detected at all tested temperatures, suggested favourable adsorption process[75].

Based on the experimental information of Table 8, the detected values of correlation coefficients (R^2) of HT-AC $_{2.5Gy}$ material showed a better significant fitting to the Langmuir model and indicated a monolayer adsorption mechanism for the AC sample treated by 2.5 Gy gamma irradiation, with

a calculated maximum monolayer adsorption capacity (q_{max}) of 970.874 mg g^{-1}. The consistency of the adsorption equilibrium data with the Langmuir isotherm indicated that, the HT-AC$_{2.5Gy}$ surface has homogenous active sites and there is a uniform distribution of the surface energy, the surface energy of HT-AC $_{2.5Gy}$ is distributed homogeneously and that single-plate adsorption occurs at 40 ppm adsorbent concentration. It can also be noted from Table 8 that, the determined R_L values for all chlorpyrifos concentrations were in the range of RL<1, which ascertained the suitability of the AC for this pesticide-type elimination. In the same context, the obtained K_L values for HT-AC and HT-AC (2.5and 5 Gy) were 0.041, 0.07 and 0.011 l/mg, which implied a higher affinity between Ictafos and AC adsorbents.

4. Recyclability and adsorption process

The activated carbon becomes saturated with the adsorbate as the adsorption process continues, which fills the sites available for adsorption. Eventually, the activated carbon 's adsorption potential decreases to a degree that makes it undesirable for further use, so it must be substituted with fresh activated carbon. There are, at least, two alternatives until carbon is depleted. It can be disposed of by incineration or land filling. In theory, or it can be regenerated[76].However, the regeneration of exhausted carbons also implies costs that, on some occasions, are not much lower than the cost of the production of new activated carbon. After a certain number of regeneration cycles, this adsorption capacity decreases to a level where the carbon cannot be regenerated anymore[77].
Regeneration process applies low temperatures (e.g., 105 °C) at the drying step, followed by high temperature pyrolysis (650 °C), and finally AC is reactivated with steam or carbon dioxide (CO2)[78]. This results in the elimination of any volatile compounds adsorbed in the carbon porosity, including residual moisture, and the thermal decomposition of other less-volatile compounds. A residue of carbonized char will stored in activated carbon pores, and become part of the structure of activated carbon[79]. The reuse of pristine activated carbon (HT-AC) and irradiated HT-AC$_{2.5Gy}$ (Highest adsorption performance) have an extremely important potential application for VOCs elimination. The adsorption efficiency of chlorpyrifos in the five cycles was presented in Figure 15. It can be noticed that, the sorption capacities of activated carbon and irradiated at 2.5Gy are gradually decreased with the increase of recyclability runs. The low adsorption capacity after recycling can be ascribed to the gradual saturation of the active sites inside the adsorbent,

resulting in an equilibrium of chlorpyrifos adsorption, Fig.15 showed that, the adsorption efficiency after five cycles of reuse (HT-AC) and (HT-AC$_{2.5Gy}$) remained at 59.6% and 76.5%, respectively. Furthermore, the mass of activated carbon has not changed significantly during adsorption and desorption. Therefore, irradiated activated carbon exhibits good sorption and recyclability for chlorpyrifos removal[80].
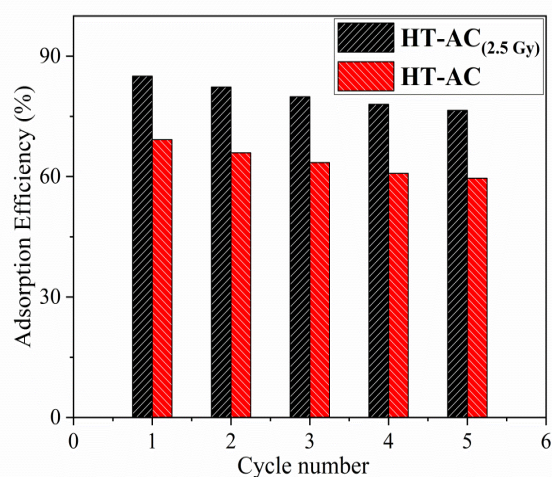

Figure 15: The adsorption efficiency after five adsorption–desorption cycles

4.1 Adsorption mechanism

As a consequence of kinetics, thermodynamics, isotherm data, the suggested mechanism of adsorption was investigated. The data showed that, it was physisorption, an exothermic process. However, it is characterized by low enthalpy values (20– 40 kJ mol-1) and Ea (kJ/mol) values were less than 40 kJ mol^{-1} as shown in Table 6. The physical interaction between the adsorbate and adsorbent can probably result from Vander Waals force, hydrogen bonding, or electrostatic force. Figure 16represents the mechanism of physical adsorption of chlorpyrifos on the surface of Activated carbon[81]

4. Conclusions

This study concluded that the activated carbon derived from a new agro-waste local source (Doum palm husk of *Hyphaene Thebaica*) is efficient adsorbent and capable of eliminating the Chlorpyrifos pesticide pollutant from ambient air. This newly developed material possessed a very high surface area with uniformly distributed active sites. The use of gamma-rays in the range of 2.5-5 gray doses for adsorption enhancement was the most convenient for modifying the physical properties of produced activated carbon and resulted in a more organized

_____

carbon-sheet structure than that of the other gamma-ray doses. In the next future, these promising results push us for developing and producing new, eco-friendly, and more highly efficient adsorbents from agro-wastes for purification of air from the VOCs pollutants. In addition, the significant ability of the formed versions of HT-AC in removing one of the VOCs harmful materials may recommend it's local use for air purification, due to availability with low cost
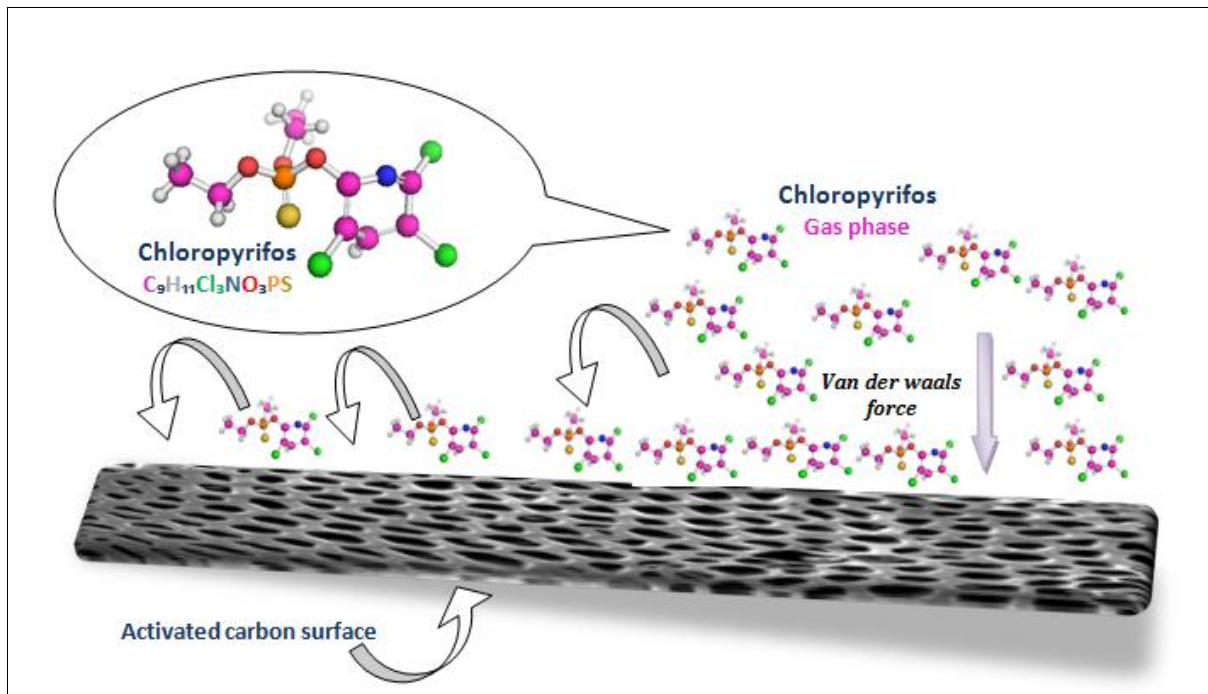

Figure 16: suggested mechanism for interaction of Chlorpyrifos with adsorbent

5. Conflicts of interest
There are no conflicts to declare.

6. Acknowledgments

7. References

[1] M. El-Sadaawy, O. Abdelwahab, Adsorptive removal of nickel from aqueous solutions by activated carbons from doum seed (Hyphaenethebaica) coat, Alexandria Engineering Journal 53(2) (2014) 399-408.

[2] R.M. Abdelhameed, M. Taha, H. Abdel-Gawad, F. Mahdy, B. Hegazi, Zeolitic imidazolate frameworks: Experimental and molecular simulation studies for efficient capture of pesticides from wastewater, Journal of Environmental Chemical Engineering 7(6) (2019) 103499.

[3] R.M. Abdelhameed, M. Taha, H. Abdel-Gawad, B. Hegazi, Amino-functionalized Al-MIL-53 for dimethoate pesticide removal from wastewater and their intermolecular interactions, Journal of Molecular Liquids 327 (2021) 114852.

[4] L. Zhao, P.-W. Xiao, Q. Chen, C. Fu, B.-H. Han, Polycarbazole and biomass-derived flexible nitrogen-doped porous carbon materials for gas adsorption and sensing, Journal of Materials Chemistry A 8(14) (2020) 6804-6811.

[5] L.K. Shrestha, R.G. Shrestha, S. Maji, B.P. Pokharel, R. Rajbhandari, R.L. Shrestha, R.R. Pradhananga, J.P. Hill, K. Ariga, High surface area nanoporous graphitic carbon materials derived from Lapsi seed with enhanced supercapacitance, Nanomaterials 10(4) (2020) 728.

[6] Q. Wang, W. Ma, E. Yin, S. Yu, S. Wang, H. Xiang, D. Li, M. Zhu, Melt-Spinning of Low-Cost Activated Carbon Fiber with Tunable Pore Structure for High-Performance Flexible Supercapacitors, ACS Applied Energy Materials (2020).

_____

[7] C.-H. Chiang, J. Chen, J.-H. Lin, Preparation of pore-size tunable activated carbon derived from waste coffee grounds for high adsorption capacities of organic dyes, Journal of Environmental Chemical Engineering (2020) 103929.

[8] S. Sekar, D.Y. Kim, S. Lee, Excellent Oxygen Evolution Reaction of Activated Carbon-Anchored NiO Nanotablets Prepared by Green Routes, Nanomaterials 10(7) (2020) 1382.

[9] S.H. Tang, M.A.A. Zaini, Development of activated carbon pellets using a facile low-cost binder for effective malachite green dye removal, Journal of Cleaner Production 253 (2020) 119970.

[10] S. Lv, Z. Zhou, M. Xue, X. Zhang, Z. Yang, Adsorption characteristics of reactive blue 81 by powdered activated carbon: Role of the calcium content, Journal of Water Process Engineering 36 (2020) 101247.

[11] C.A. Okonkwo, G. Li, Y. Li, T. Lv, L. Jia, C.C. Okoye, S.N. Oba, Liquid nitrogen-controlled direct pyrolysis/KOH activation mediated micro-mesoporous carbon synthesis from castor shell for enhanced performance of supercapacitor electrode, Biomass Conversion and Biorefinery (2021) 1-12.

[12] N. Panwar, A. Pawar, Influence of activation conditions on the physicochemical properties of activated biochar: a review, Biomass Conversion and Biorefinery (2020) 1-23.

[13] J. Bai, Q. Lu, Q. Zhao, J. Wang, Z. Gao, G. Zhang, Organochlorine pesticides (OCPs) in wetland soils under different land uses along a 100-year chronosequence of reclamation in a Chinese estuary, Scientific reports 5 (2015) 17624.

[14] R. Abdelhameed, H. Abdel-Gawad, C. Silva, J. Rocha, B. Hegazi, A. Silva, Kinetic and equilibrium studies on the removal of 14 C-ethion residues from wastewater by copper-based metal–organic framework, International Journal of Environmental Science and Technology 15(11) (2018) 2283-2294.

[15] H. Abdel-Gawad, L. Afifi, R. Abdel-Hameed, B. Hegazi, Distribution and degradation of 14C-ethyl prothiofos in a potato plant and the effect of processing, Phosphorus, Sulfur, and Silicon and the Related Elements 183(11) (2008) 2734-2751.

[16] S. Das, K.J. Hageman, M. Taylor, S. Michelsen-Heath, I. Stewart, Fate of the organophosphate insecticide, chlorpyrifos, in leaves, soil, and air following application, Chemosphere 243 (2020) 125194.

[17] J. Lalah, D. Ondieki, S. Wandiga, I. Jumba, Dissipation, distribution, and uptake of 14 C-chlorpyrifos in a model tropical seawater/sediment/fish ecosystem, Bulletin of environmental contamination and toxicology 70(5) (2003) 0883-0890.

[18] R.M. Abdelhameed, H. Abdel-Gawad, H.E. Emam, Macroporous Cu-MOF@ cellulose acetate membrane serviceable in selective removal of dimethoate pesticide from wastewater, Journal of Environmental Chemical Engineering 9(2) (2021) 105121.

[19] M. Leistra, J.H. Smelt, J.H. Weststrate, F. van den Berg, R. Aalderink, Volatilization of the pesticides chlorpyrifos and fenpropimorph from a potato crop, Environmental science & technology 40(1) (2006) 96-102.

[20] P. Sarker, S.K. Sen, M. Mia, M. Pervez, A. Mortuza, S. Hossain, M. Mortuza, M. Ali, S. Nur, H. Kabir, Effect of gamma irradiation on structural, morphological and optical properties of thermal spray pyrolysis deposited CuO thin film, Ceramics International 47(3) (2021) 3626-3633.

[21] A. Ahmad, G. El-Shobaky, A. Al-Noaimi, H. El-Shobaky, Surface and catalytic properties of gamma-irradiated CuO and NiO catalysts, Materials Letters 26(1-2) (1996) 107-112.

[22] I. Kellartzis, E. Kokkinos, G. Stavropoulos, A. Zouboulis, M. Mitrakas, Techno-economic evaluation of tetravalent manganese feroxyhyte for Hg uptake from flue gases in a fixed-bed adsorption configuration, Journal of environmental chemical engineering 5(2) (2017) 2077-2082.

[23] K.R. Solomon, W.M. Williams, D. Mackay, J. Purdy, J.M. Giddings, J.P. Giesy, Properties and uses of chlorpyrifos in the United States, Ecological risk assessment for chlorpyrifos in terrestrial and aquatic systems in the United States (2014) 13-34.

[24] E. Liakos, K. Rekos, D. Giannakoudakis, A. Mitropoulos, G. Kyzas, Carbonaceous Adsorbents Derived from Agricultural Sources for the Removal of Pramipexole Pharmaceutical Model Compound from Synthetic Aqueous Solutions. Processes 2021, 9, 253, s Note: MDPI stays neutral with regard to jurisdictional claims in published …, 2021.

[25] A. Lamplugh, M. Harries, A. Nguyen, L. Montoya, VOC emissions from nail salon products and their effective removal using affordable adsorbents and synthetic jets, Building and Environment 168 (2020) 106499.

[26] R. Sato, K. Tanaka, H. Ishida, S. Koguchi, J.P. Ramos Ramirez, H. Matsukura, H. Ishida, Detection of gas drifting near the ground by

drone hovering over: Using airflow generated by two connected quadcopters, Sensors 20(5) (2020) 1397.

[27] S. Kutluay, O. Baytar, Ö. Şahin, Equilibrium, kinetic and thermodynamic studies for dynamic adsorption of benzene in gas phase onto activated carbon produced from elaeagnus angustifolia seeds, Journal of Environmental Chemical Engineering 7(2) (2019) 102947.

[28] F. Suarez-Garcia, A. Martinez-Alonso, J. Tascon, Pyrolysis of apple pulp: effect of operation conditions and chemical additives, Journal of Analytical and Applied Pyrolysis 62(1) (2002) 93-109.

[29] B. Sakintuna, Y. Yürüm, S. Çetinkaya, Evolution of carbon microstructures during the pyrolysis of Turkish Elbistan lignite in the temperature range 700– 1000 C, Energy & fuels 18(3) (2004) 883-888.

[30] N. Yoshizawa, K. Maruyama, Y. Yamada, M. Zielinska-Blajet, XRD evaluation of CO2 activation process of coal-and coconut shell-based carbons, Fuel 79(12) (2000) 1461-1466.

[31] V.S. Babu, M. Seehra, Modeling of disorder and X-ray diffraction in coal-based graphitic carbons, Carbon 34(10) (1996) 1259-1265.

[32] B.S. Girgis, A.-N.A. El-Hendawy, Porosity development in activated carbons obtained from date pits under chemical activation with phosphoric acid, Microporous and mesoporous materials 52(2) (2002) 105-117.

[33] M. Jagtoyen, F. Derbyshire, Activated carbons from yellow poplar and white oak by H3PO4 activation, Carbon 36(7-8) (1998) 1085-1097.

[34] C. Ishii, K. Kaneko, Surface and physical properties of microporous carbon spheres, Progress in organic coatings 31(1-2) (1997) 147-152.

[35] B.S. Girgis, Y.M. Temerk, M.M. Gadelrab, I.D. Abdullah, X-ray diffraction patterns of activated carbons prepared under various conditions, Carbon letters 8(2) (2007) 95-100.

[36] D. Prahas, Y. Kartika, N. Indraswati, S. Ismadji, Activated carbon from jackfruit peel waste by H3PO4 chemical activation: Pore structure and surface chemistry characterization, Chemical Engineering Journal 140(1-3) (2008) 32-42.

[37] R. Abdelhameed, F. Mahdy, H. Abdel-Gawad, B. Hegazi, Green process for adsorptive removal of ethion (O, O, O', O'-tetraethyl S, S'-methylene bis (phosphorodithioate) from agricultural wastewater using modified surface of orange peel and apricot kernel, Egyptian Journal of Chemistry 63(10) (2020) 2-3.

[38] S. Gao, L. Zhu, L. Liu, A. Gao, F. Liao, M. Shao, Improved Energy Storage Performance Based on Gamma-Ray Irradiated Activated Carbon Cloth, Electrochimica Acta 191 (2016) 908-915.

[39] M. Rahman, M. Muttakin, A. Pal, A.Z. Shafiullah, B.B. Saha, A Statistical Approach to Determine Optimal Models for IUPAC-Classified Adsorption Isotherms, Energies 12(23) (2019) 4565.

[40] S. Yakout, G.S. El-Deen, Characterization of activated carbon prepared by phosphoric acid activation of olive stones, Arabian journal of chemistry 9 (2016) S1155-S1162.

[41] A. Kumar, H.M. Jena, Preparation and characterization of high surface area activated carbon from Fox nut (Euryale ferox) shell by chemical activation with H3PO4, Results in Physics 6 (2016) 651-658.

[42] H.N. Tran, F.-C. Huang, C.-K. Lee, H.-P. Chao, Activated carbon derived from spherical hydrochar functionalized with triethylenetetramine: synthesis, characterizations, and adsorption application, Green Processing and Synthesis 6(6) (2017) 565-576.

[43] B. Zhao, P. Liu, Y. Jiang, D. Pan, H. Tao, J. Song, T. Fang, W. Xu, Supercapacitor performances of thermally reduced graphene oxide, Journal of power sources 198 (2012) 423-427.

[44] A. Geczo, D.A. Giannakoudakis, K. Triantafyllidis, M.R. Elshaer, E. Rodríguez-Aguado, S. Bashkova, Mechanistic insights into acetaminophen removal on cashew nut shell biomass-derived activated carbons, Environmental Science and Pollution Research (2020) 1-14.

[45] A. Puziy, O. Poddubnaya, A. Martınez-Alonso, F. Suárez-Garcıa, J. Tascón, Synthetic carbons activated with phosphoric acid: I. Surface chemistry and ion binding properties, Carbon 40(9) (2002) 1493-1505.

[46] G. Socrates, Infrared characteristic frequencies: tables and charts, Chichester (1994).

[47] F. Derbyshire, Catalysis in direct coal liquefaction: status and directions for research, Prepr. Pap., Am. Chem. Soc., Div. Fuel Chem.;(United States) 33(CONF-8809273-) (1988).

[48] A. Puziy, O. Poddubnaya, A. Martínez-Alonso, F. Suárez-García, J. Tascón, Characterization of synthetic carbons activated with phosphoric acid, Applied surface science 200(1-4) (2002) 196-202.

[49] X. Zhou, X. Qu, R. Zhang, J. Bi, Study of the microtextural transformation of coal char during supercritical water activation, Fuel Processing Technology 135 (2015) 195-202.

[50] S. Yao, J. Zhang, D. Shen, R. Xiao, S. Gu, M. Zhao, J. Liang, Removal of Pb (II) from water by the activated carbon modified by nitric acid under microwave heating, Journal of Colloid and Interface Science 463 (2016) 118-127.

[51] W. Lu, M. Liu, L. Miao, D. Zhu, X. Wang, H. Duan, Z. Wang, L. Li, Z. Xu, L. Gan, Nitrogen-containing ultramicroporous carbon nanospheres for high performance supercapacitor electrodes, Electrochimica Acta 205 (2016) 132-141.

[52] A.C. Ferrari, Raman spectroscopy of graphene and graphite: Disorder, electron–phonon coupling, doping and nonadiabatic effects, Solid state communications 143(1-2) (2007) 47-57.

[53] S. Ryu, L. Liu, S. Berciaud, Y.-J. Yu, H. Liu, P. Kim, G.W. Flynn, L.E. Brus, Atmospheric oxygen binding and hole doping in deformed graphene on a SiO2 substrate, Nano letters 10(12) (2010) 4944-4951.

[54] A. Ansón-Casaos, J. Puértolas, F.J. Pascual, J. Hernández-Ferrer, P. Castell, A.M. Benito, W.K. Maser, M. Martínez, The effect of gamma-irradiation on few-layered graphene materials, Applied Surface Science 301 (2014) 264-272.

[55] V. Krishnakumar, D. Avasthi, F. Singh, P. Kulriya, R. Nagalakshmi, Study of the damage produced in K [CS (NH2) 2] 4Br–a non-linear optical single crystal by swift heavy ion irradiation, Nuclear Instruments and Methods in Physics Research Section B: Beam Interactions with Materials and Atoms 256(2) (2007) 675-682.

[56] L.H. Isherwood, G. Athwal, B.F. Spencer, C. Casiraghi, A. Baidak, Gamma Radiation-Induced Oxidation, Doping, and Etching of Two-Dimensional MoS2 Crystals, The Journal of Physical Chemistry C 125(7) (2021) 4211-4222.

[57] M. Ahlam, M. Ravishankar, N. Vijayan, G. Govindaraj, A.G. Prakash, Investigation of gamma radiation effect on chemical properties and surface morphology of some nonlinear optical (NLO) single crystals, Nuclear Instruments and Methods in Physics Research Section B: Beam Interactions with Materials and Atoms 278 (2012) 26-33.

[58] I. Velo-Gala, J.J. Lopez-Penalver, M. Sanchez-Polo, J. Rivera-Utrilla, Surface modifications of activated carbon by gamma irradiation, Carbon 67 (2014) 236-249.

[59] T. Kanagasekaran, P. Mythili, P. Srinivasan, N. Vijayan, D. Kanjilal, R. Gopalakrishnan, P. Ramasamy, On the observation of physical, chemical, optical and thermal changes induced by 50 MeV silicon ion in benzimidazole single crystals, Materials Research Bulletin 43(4) (2008) 852-863.

[60] A. Hassan, A. Abdel-Mohsen, M.M. Fouda, Comparative study of calcium alginate, activated carbon, and their composite beads on methylene blue adsorption, Carbohydrate polymers 102 (2014) 192-198.

[61] A.A. Inyinbor, F.A. Adekola, G.A. Olatunji, Copper scavenging efficiency of adsorbents prepared from Raphia hookeri fruit waste, Sustainable Chemistry and pharmacy 12 (2019) 100141.

[62] A. Fahmy, A. Elzaref, H. Youssef, H. Shehata, M. Wassel, J. Friedrich, F. Poncin-Epaillard, D. Debarnot, Plasma O $_{2}$ modifies the structure of synthetic zeolite-A to improve the removal of cadmium ions from aqueous solutions, Turkish Journal of Chemistry 43(1) (2019) 172-184.

[63] R.M. Abdelhameed, H. Abdel-Gawad, B. Hegazi, Effective adsorption of prothiofos (O-2, 4-dichlorophenyl O-ethyl S-propyl phosphorodithioate) from water using activated agricultural waste microstructure, Journal of Environmental Chemical Engineering 8(3) (2020) 103768.

[64] J. Yang, M. Yu, W. Chen, Adsorption of hexavalent chromium from aqueous solution by activated carbon prepared from longan seed: Kinetics, equilibrium and thermodynamics, Journal of industrial and engineering chemistry 21 (2015) 414-422.

[65] M.S. Yahia, A.S. Elzaref, M.B. Awad, A.M. Tony, A.S. Elfeky, Efficient adsorption of chlorpyrifos onto modified activated carbon by gamma irradiation; a plausible adsorption mechanism, Zeitschrift für Physikalische Chemie (000010151520201765) (2021).

[66] M. Ahmad, S.S. Lee, S.-E. Oh, D. Mohan, D.H. Moon, Y.H. Lee, Y.S. Ok, Modeling adsorption kinetics of trichloroethylene onto biochars derived from soybean stover and peanut shell wastes, Environmental Science and Pollution Research 20(12) (2013) 8364-8373.

[67] S. Nethaji, A. Sivasamy, R.V. Kumar, A. Mandal, Preparation of char from lotus seed biomass and the exploration of its dye removal capacity through batch and column adsorption studies, Environmental Science and Pollution Research 20(6) (2013) 3670-3678.

[68] W.J. Weber, J.C. Morris, Kinetics of adsorption on carbon from solution, Journal of the sanitary engineering division 89(2) (1963) 31-60.

_____

[69] E. Holley, Diffusion and boundary layer concepts in aeration through liquid surfaces, Water Research 7(4) (1973) 559-573.

[70] E.C. Lima, A. Hosseini-Bandegharaei, J.C. Moreno-Piraján, I. Anastopoulos, A critical review of the estimation of the thermodynamic parameters on adsorption equilibria. Wrong use of equilibrium constant in the Van't Hoof equation for calculation of thermodynamic parameters of adsorption, Journal of Molecular Liquids 273 (2019) 425-434.

[71] M. Horsfall Jnr, A.I. Spiff, Effects of temperature on the sorption of Pb2+ and Cd2+ from aqueous solution by Caladium bicolor (Wild Cocoyam) biomass, Electronic Journal of Biotechnology 8(2) (2005) 43-50.

[72] T. Anirudhan, P. Radhakrishnan, Thermodynamics and kinetics of adsorption of Cu (II) from aqueous solutions onto a new cation exchanger derived from tamarind fruit shell, The Journal of Chemical Thermodynamics 40(4) (2008) 702-709.

[73] C. Tang, Y. Shu, R. Zhang, X. Li, J. Song, B. Li, Y. Zhang, D. Ou, Comparison of the removal and adsorption mechanisms of cadmium and lead from aqueous solution by activated carbons prepared from Typha angustifolia and Salix matsudana, RSC advances 7(26) (2017) 16092-16103.

[74] A.S. Elfeky, H.F. Youssef, A.S. Elzaref, Adsorption of dye from wastewater onto ZnO nanoparticles-loaded zeolite: Kinetic, thermodynamic and isotherm studies, Zeitschrift für Physikalische Chemie 234(2) (2020) 255-278.

[75] M.E. Peñafiel, J.M. Matesanz, E. Vanegas, D. Bermejo, R. Mosteo, M.P. Ormad, Comparative adsorption of ciprofloxacin on sugarcane bagasse from Ecuador and on commercial powdered activated carbon, Science of The Total Environment 750 (2021) 141498.

[76] S.Y. Hwang, G.B. Lee, J.H. Kim, B.U. Hong, J.E. Park, Pre-Treatment Methods for Regeneration of Spent Activated Carbon, Molecules 25(19) (2020) 4561.

[77] A. Larasati, G.D. Fowler, N.J. Graham, Chemical regeneration of granular activated carbon: preliminary evaluation of alternative regenerant solutions, Environmental Science: Water Research & Technology 6(8) (2020) 2043-2056.

[78] B. Sonmez Baghirzade, Y. Zhang, J.F. Reuther, N.B. Saleh, A.K. Venkatesan, O.G. Apul, Thermal Regeneration of Spent Granular Activated Carbon Presents an Opportunity to Break the Forever PFAS Cycle, Environmental Science & Technology 55(9) (2021) 5608-5619.

[79] Y. Guo, E. Du, The effects of thermal regeneration conditions and inorganic compounds on the characteristics of activated carbon used in power plant, Energy Procedia 17 (2012) 444-449.

[80] K. Shen, M. Gondal, Removal of hazardous Rhodamine dye from water by adsorption onto exhausted coffee ground, Journal of Saudi Chemical Society 21 (2017) S120-S127.

[81] A. Görgülü, H. Yağlı, Y. Koç, A. Koç, N.A. Öztürk, Ö. Köse, Experimental study of butane adsorption on coconut based activated carbon for different gas concentrations, temperatures and relative humidities, Environmental technology 42(14) (2021) 2122-2131.

_____